doi:10.1093/brain/aww351 BRAIN 2017: 140; 599–616 | 599

BRAIN
A JOURNAL OF NEUROLOGY

Gene therapy targeting oligodendrocytes provides therapeutic benefit in a leukodystrophy model

Elena Georgiou,[1] Kyriaki Sidiropoulou,[2] Jan Richter,[3] Christos Papaneophytou,[1] Irene Sargiannidou,[1] Alexia Kagiava,[1] Georg von Jonquieres,[4] Christina Christodoulou,[3] Matthias Klugmann[4] and Kleopas A. Kleopa[1,5]

Pelizaeus-Merzbacher-like disease or hypomyelinating leukodystrophy-2 is an autosomal recessively inherited leukodystrophy with childhood onset resulting from mutations in the gene encoding the gap junction protein connexin 47 (Cx47, encoded by *GJC2*). Cx47 is expressed specifically in oligodendrocytes and is crucial for gap junctional communication throughout the central nervous system. Previous studies confirmed that a cell autonomous loss-of-function mechanism underlies hypomyelinating leukodystrophy-2 and that transgenic oligodendrocyte-specific expression of another connexin, Cx32 (*GJB1*), can restore gap junctions in oligodendrocytes to achieve correction of the pathology in a disease model. To develop an oligodendrocyte-targeted gene therapy, we cloned the *GJC2*/Cx47 gene under the myelin basic protein promoter and used an adeno-associated viral vector (AAV.MBP.Cx47myc) to deliver the gene to postnatal Day 10 mice via a single intracerebral injection in the internal capsule area. Lasting Cx47 expression specifically in oligodendrocytes was detected in Cx47 single knockout and Cx32/Cx47 double knockout mice up to 12 weeks post-injection, including the corpus callosum and the internal capsule but also in more distant areas of the cerebrum and in the spinal cord. Application of this oligodendrocyte-targeted somatic gene therapy at postnatal Day 10 in groups of double knockout mice, a well characterized model of hypomyelinating leukodystrophy-2, resulted in significant improvement in motor performance and coordination at 1 month of age in treated compared to mock-treated mice, as well as prolonged survival. Furthermore, immunofluorescence and morphological analysis revealed improvement in demyelination, oligodendrocyte apoptosis, inflammation, and astrogliosis, all typical features of this leukodystrophy model in both brain and spinal cord. Functional dye transfer analysis confirmed the re-establishment of oligodendrocyte gap junctional connectivity in treated as opposed to untreated mice. These results provide a significant advance in the development of oligodendrocyte-cell specific gene therapy. Adeno-associated viral vectors can be used to target therapeutic expression of a myelin gene to oligodendrocytes. We show evidence for the first somatic gene therapy approach to treat hypomyelinating leukodystrophy-2 preclinically, providing a potential treatment for this and similar forms of leukodystrophies.

1 Neuroscience Laboratory, The Cyprus Institute of Neurology and Genetics and Cyprus School of Molecular Medicine, Nicosia, Cyprus
2 Department of Zoology, University of Crete, Heraklion, Greece
3 Department of Molecular Virology, The Cyprus Institute of Neurology and Genetics and Cyprus School of Molecular Medicine, Nicosia, Cyprus
4 Translational Neuroscience Facility and Department of Physiology, School of Medical Sciences, University of New South Wales, Sydney, Australia
5 Neurology Clinics, The Cyprus Institute of Neurology and Genetics and Cyprus School of Molecular Medicine, Nicosia, Cyprus

Correspondence to: Kleopas A. Kleopa, MD
The Cyprus Institute of Neurology and Genetics
6 International Airport Avenue, P.O. Box 23462,
1683, Nicosia, Cyprus
E-mail: kleopa@cing.ac.cy

Received May 12, 2016. Revised November 22, 2016. Accepted November 28, 2016. Advance Access publication January 18, 2017

Keywords: leukodystrophy; connexin; gap junctions; myelin basic protein promoter; AAV, gene therapy

Abbreviations: AAV = adeno-associated virus; HLD2 = hypomyelinating leukodystrophy-2

Introduction

Pelizaeus-Merzbacher disease is an X-linked disorder caused by mutations in *PLP1*, the gene encoding proteolipid protein, the main protein in CNS myelin. Classic Pelizaeus-Merzbacher disease affects boys and is characterized by nystagmus and impaired psychomotor development within the first year of life, followed by progressive spasticity, ataxia, choreoathetosis and diffuse white matter changes on MRI (Nave and Boespflug-Tanguy, 1996; Hudson *et al.*, 2004; Inoue, 2005). *PLP1* mutations may also cause a more severe 'connatal' Pelizaeus-Merzbacher disease phenotype, as well as a milder disease, hereditary spastic paraplegia (HSP) type 2 (Garbern *et al.*, 1999; Hudson *et al.*, 2004; Garbern, 2007). Pelizaeus-Merzbacher-like disease 1 (PMLD1)/hypomyelinating leukodystrophy-2 (HLD2) (OMIM #608804), which is not associated with *PLP1* mutations, usually presents with nystagmus by 7 weeks of age, impaired motor development and ataxia by 15 months, evidence of hypomyelination on MRI, and later development of spasticity. Different homozygous and compound heterozygous *GJA12/GJC2* mutations affecting the gap junction protein connexin 47 (Cx47) were identified in consanguineous and non-consanguineous families with autosomal recessive inheritance (Uhlenberg *et al.*, 2004; Bugiani *et al.*, 2006). Homozygous deletions leading to frameshift in the *GJA12/GJC2* gene were also reported to cause a similar phenotype (Salviati *et al.*, 2007; Wolf *et al.*, 2007), suggesting a loss-of-function effect. As with *PLP1* mutations, the phenotypic spectrum of *GJA12/GJC2* mutations has been expanded to include a late-onset, slowly progressive, complicated spastic paraplegia, with normal or near-normal psychomotor development, preserved walking capability through adulthood, and no nystagmus (Orthmann-Murphy *et al.*, 2009). Thus, *GJA12/GJC2* mutations, like *PLP1* mutations, can result in a milder phenotype than leukodystrophy.

Cx47 (encoded by *GJC2*) is one of the two gap junction proteins forming intercellular channels in oligodendrocytes along with Cx32 (*GJB1*) (Rash *et al.*, 2001; Altevogt and Paul, 2004). It is localized in the perikarya and proximal processes of all oligodendrocytes (Menichella *et al.*, 2003; Odermatt *et al.*, 2003; Kleopa *et al.*, 2004), forming homotypic oligodendrocyte-oligodendrocyte or heterotypic oligodendrocyte-astrocyte gap junctions with Cx43 as astrocytic partner (Altevogt and Paul, 2004; Kamasawa *et al.*, 2005; Orthmann-Murphy *et al.*, 2007*b*, 2009). Cx32 is mainly expressed along large myelinated fibres of the white matter (Altevogt *et al.*, 2002; Kleopa *et al.*, 2004), forming intracellular gap junctions within the myelin sheath but also in cell bodies of mainly grey matter oligodendrocytes forming oligodendrocyte-astrocyte gap junctions with Cx30 as astrocytic partner (Rash *et al.*, 2001; Nagy *et al.*, 2003; Altevogt and Paul, 2004; Kamasawa *et al.*, 2005). A third connexin, Cx29 and its human orthologue Cx31.3 form only hemichannels along thin myelinated fibres (Kleopa *et al.*, 2004; Ahn *et al.*, 2008; Sargiannidou *et al.*, 2008).

HLD2-associated mutations result in loss-of-function of Cx47 when expressed in a mammalian cell line (Orthmann-Murphy *et al.*, 2007*a*). Unlike wild-type Cx47, these mutants were at least partially retained in the endoplasmic reticulum and failed to form functional homotypic channels. Thus, they cause the HLD2 phenotype most likely by interfering with the normal function of Cx47/Cx43 channels. Indeed, all three missense mutants failed to form functional Cx47/Cx43 channels (Orthmann-Murphy *et al.*, 2007*b*).

Deletion of the *Gjc2/Cx47* gene in Cx47 knockout mice results in only mild CNS pathology, likely due to the compensatory function of Cx32, which is not sufficient in humans. Likewise, deletion of *Gjb1/Cx32* in Cx32 knockout mice results in very mild CNS myelination defects (Sutor *et al.*, 2000; Sargiannidou *et al.*, 2009). However, deletion of both major oligodendrocyte connexins in the Cx32/Cx47 double knockout mouse causes severe and early onset CNS demyelination since oligodendrocytes are deprived of gap junctional communication completely. These mice present with a coarse action tremor during the third postnatal week that worsens over time, followed by tonic seizures during the fourth to fifth postnatal week. The seizures increase in frequency and severity until the animals die, typically during the sixth postnatal week (Menichella *et al.*, 2003; Odermatt *et al.*, 2003). Pathologically, double knockout mice show dys/hypomyelination followed by early demyelination. Delayed myelination in the optic nerve is evident already at postnatal Day 7, while at postnatal Days 14–21 thin myelin sheaths and vacuolation are present (Menichella *et al.*, 2003). At 1 month of age, double knockout mice exhibit severe CNS demyelination, axonal degeneration and oligodendrocyte apoptosis in the spinal cord funiculi and in the optic nerve. Besides thinner myelin sheaths they show oedematous extracellular spaces separating degenerating axons from their myelin sheath (Menichella *et al.*, 2003; Odermatt *et al.*, 2003). Thus, Cx32/Cx47 double knockout mice provide a relevant mouse model of early onset hypomyelinating leukodystrophy as seen in patients with HLD2 and can be harnessed to test future therapies.

Based on the molecular-genetic mechanism of HLD2, we examined the possibility of a gene therapy approach by delivering the human *GJC2*/Cx47 gene specifically to oligodendrocytes of Cx32/Cx47 double knockout mice. To develop an oligodendrocyte-targeted gene delivery we used a

chimeric AAV1/2 vector previously shown to efficiently infect oligodendrocytes (von Jonquieres *et al.*, 2013) carrying the *GJC2*/Cx47 gene under the control of the 1.9 kb oligodendrocyte-specific myelin basic protein (MBP) promoter and established a gene delivery approach in postnatal Day 10 mice. A treatment trial in double knockout mice showed a significant therapeutic benefit in treated compared to mock-treated or untreated mice at 1 month of age by re-establishing oligodendrocyte gap junction connectivity and rescuing the severe demyelination in this model of HLD2.

Materials and methods

Animals

C57BL/6 mice (wild-type) as well as *Gjb1*-null/Cx32 knockout mice (C57BL/6_129) (Nelles *et al.*, 1996) and *Gjc2*/Cx47 knockout mice (C57BL/6;129P2/OlaHsd) (Odermatt *et al.*, 2003), both obtained from the European Mouse Mutant Archive, Monterotondo, Italy (originally generated by Prof. Klaus Willecke, University of Bonn) were kept in our mouse facility under specific pathogen-free, standard controlled conditions of temperature (21–23°C), humidity, air exchange and light cycle (12/12 h light/dark) and provided with standardized mouse diet and drinking water *ad libitum*. Cx32KO/Cx47Het mice were obtained by breeding Cx32 knockout female mice with Cx47 knockout male mice, and double knockout mice were obtained by further breeding between heterozygous mice. Genotypes were confirmed by simultaneous polymerase chain reaction (PCR) screening as previously described (Schiza *et al.*, 2015). Cx47 knockout mice as well as double knockout mice derived from them express transgenically EGFP in all oligodendrocytes (Odermatt *et al.*, 2003). For the dye transfer studies we also used as positive controls TG + Cx32/Cx47 double knockout mice that have transgenically established gap junction connectivity in green fluorescent oligodendrocytes (Schiza *et al.*, 2015). All animal procedures were approved by the Government's Chief Veterinary Officer according to EU guidelines (EC Directive 86/609/EEC).

Adeno-associated virus vector cloning

The adeno-associated virus (AAV) construct pAM/MBP-EGFP-WPRE-bGH (von Jonquieres *et al.*, 2013), containing the woodchuck hepatitis virus post-transcriptional regulatory element (WPRE) and the bovine growth hormone polyadenylation sequence (bGHpA) flanked by AAV2 inverted terminal repeats was used to generate the final pMBP-Cx47myc plasmid. The myc tag was added to the Cx47 open reading frame (ORF) to provide an additional marker for confirming expression, because commercially available Cx47 antibodies showed non-specific binding in Cx47 knockout mice in our previous studies as also reported by others (May *et al.*, 2013). We PCR-amplified XhoI-Cx47myc-HindIII from the pIRES2-EGFP-Cx47 (Orthmann-Murphy *et al.*, 2007*a*) using the primers Cx47myc-F (CCGCTCGAGATGAGCTGGAGCTTCCTG) and Cx47myc-R (CCCAAGCTTTTACAGGTCCTCCTCGCTGATCAGCTTCTGCTCGATCCACACGGTGGTCTTCCCG-T) to introduce the myc tag. The amplified product was then digested using XhoI/HindIII and inserted into the pAM/MBP-EGPP-WPRE that has also been digested with XhoI/HindIII, to obtain the pAM/MBP-Cx47myc-WPRE construct. The proximal 1.9 kb *Mbp* promoter shown to drive expression in oligodendrocytes (Forghani *et al.*, 2001) was PCR-amplified, digested with KpnI/XhoI and ligated into pAM/MBP-Cx47myc-WPRE to obtain the final construct pAM/MBP-Cx47myc-WPRE (hereafter referred to as AAV.MBP.Cx47 myc, or full AAV plasmid), while the original AAV.MBP .EGFP plasmid (von Jonquieres *et al.*, 2013) was used as control (also referred to as AAV.MBP.mock or mock AAV plasmid) for all expression and treatment studies (Fig. 1A and B).

Adeno-associated virus vector production and titration

The production of chimeric AAV1/2 vectors was performed according to the published methods (von Jonquieres *et al.*, 2013). Briefly, AAV-293 cells (Agilent Technologies) were co-transfected with the vector plasmid (containing the transgene cassette and AAV inverted terminal repeats), the serotype-specific AAV helper plasmids, pH 21 and pRV-1, encoding *rep* and *cap* genes of AAV1 and AAV2, respectively, and the adenovirus helper plasmid (pFΔ6), by standard $CaPO_4$ transfection. Cells were harvested 60 h after transfection and vectors were purified using HiTrap™ heparin affinity columns (Sigma). Purified vector was concentrated using Amicon® ultra-4 centrifugal filter units with a 100 K molecular weight cut-off to a volume of 250 µl. The concentrator was rinsed with an equal volume of phosphate-buffered saline (PBS), and solutions were pooled and sterile filtered. Vector genome titres were determined by quantitative PCR using the TaqMan® Universal PCR Master Mix (ThermoFisher Scientific) with primers and probe targeting the WPRE. In addition, vector particle titres were determined using the Progen AAV2 titration ELISA (PRATV, Progen Biotechnik), an enzyme immunoassay utilizing a capture-antibody that detects a conformational epitope not present on unassembled capsid proteins.

Establishment of adeno-associated virus vector delivery to postnatal Day 10 mouse brain

Based on recent observations that neonatal (postnatal Days 1–2) delivery of the *Mbp* promoter driven vectors (AAV and lentiviral) causes some expression in other cell types besides oligodendrocytes (von Jonquieres *et al.*, 2013; Kagiava *et al.*, 2014), we modified the injection protocol to deliver the AAV.MBP vectors at postnatal Day 10, when selectivity for oligodendrocyte cell linage is much higher (von Jonquieres *et al.*, 2013). The time point of the injection was set early enough in order to prevent severe demyelination, which normally begins during the fourth week of life (after postnatal Day 20) in Cx32/Cx47 double knockout mice (Menichella *et al.*, 2003; Odermatt *et al.*, 2003), the leukodystrophy model we used for the gene therapy treatment study.

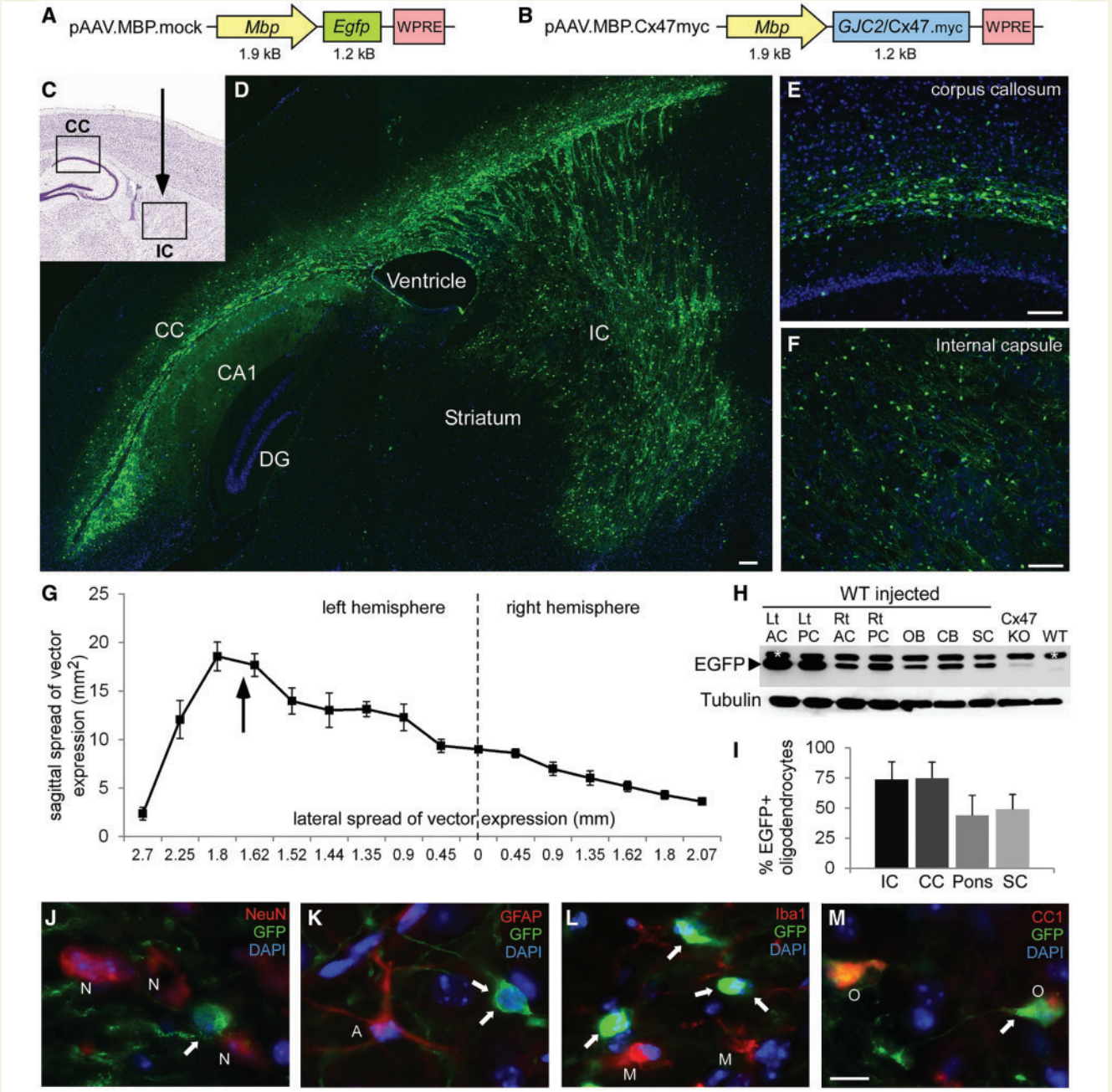

Figure 1 AAV vectors and EGFP expression in the CNS of AAV.MBP.EGFP injected mice. Schematic diagrams of the AAV.MBP.EGFP (mock) (**A**) and AAV.MBP.Cx47myc (**B**) vector plasmids used in this study. Injection of the mock vector in the internal capsule (IC) of wild-type (WT) postnatal Day 10 (P10) mice (indicated by arrow in the diagram in **C**) resulted in widespread expression in the internal capsule as well as the corpus callosum (CC). Composition of low magnification images from a sagittal section in **D**, as well as higher magnification images of the corpus callosum (**E**) and internal capsule (**F**) demonstrate the extend of AAV-derived reporter gene EGFP expression in oligodendrocytes (green). Cell nuclei are counterstained with DAPI (blue). (**G**) Quantification of expression volume in both hemispheres from sagittal brain sections taken from $n = 5$ injected mice. Arrow shows the level of the vector injection in the internal capsule of the left hemisphere. (**H**) Immunoblot analysis of EGFP expression in lysates from different CNS areas of an AAV.MBP.EGFP-injected wild-type mouse, including left (Lt) and right (Rt) anterior and posterior cerebrum (AC and PC), olfactory bulb (OB), cerebellum (CB), and spinal cord (SC) shows widespread expression with higher levels in the injected left hemisphere. A brain sample from Cx47 knockout mouse (transgenically expressing EGFP) shows lower levels of EGFP. A non-injected wild-type mouse brain is shown as negative control. A non-specific band is present (marked with asterisk) above the specific band for EGFP. Tubulin blot is shown underneath as loading control. (**I**) Quantification of the percentage of EGFP expressing oligodendrocytes in the corpus callosum, internal capsule, ventral pons (corticospinal tract area) and cervical spinal cord (SC) anteriolateral white matter of $n = 5$ mice shows high expression ratios in all areas, although lower in pons and spinal cord. (**J–M**) Immunostaining with cell markers as indicated confirms that AAV.MBP.EGFP expression (arrows) is not present in NeuN + neurons (N), in GFAP + astrocytes (A), or in Iba1 + microglia (M), but is localized only in CC1 + oligodendrocytes (O). DG = dentate gyrus.

Postnatal Day 10 mice (C57BL/6 mice for AAV.MBP.mock and Cx47 knockout or Cx32/Cx47 double knockout mice for AAV.MBP.Cx47myc vectors) were anaesthetized with avertin before the injection procedure and were placed onto a stereotaxic frame (Kopf instruments) using an adaptor. Five to 15 µl of the vector solution was injected into the internal capsule (+4.0 mm AP, 1.7 mm ML, −3 mm DV from lambda). Vector delivery was performed at a rate of 150 nl/min with a 34G Hamilton syringe. The needle was left in place for 5 min prior to slowly retracting it from the brain. Following injections, the pups were left on a 37°C warm-plate to recover their mobility, returned to their mother as a group and observed until postnatal Day 30 or until death (double knockout mice) for the treatment study, or up to 3 months (Cx47 knockout), to assess duration of expression.

Tissue processing and analysis of transgene expression

The expression of the AAV.MBP.EGFP mock vector was assessed through EGFP detection mainly by green fluorescence or by immunohistochemistry 20 days post-injection (dpi), corresponding to postnatal Day 30. In AAV.MBP.Cx47myc injected mice we analysed Cx47 expression using antibodies against Cx47 or against the myc tag. For both EGFP and Cx47 expression, the identity of expressing cells was examined by double immunostaining with cell markers including GFAP (astrocytes), CC-1 (oligodendrocytes), NeuN (neurons), or Iba1 (microglia).

For immunostaining, mice were anaesthetized intraperitoneally with Avertin® and then transcardially perfused with PBS followed by fresh 4% paraformaldehyde. Brain and cervicothoracic spinal cord tissues were harvested and further fixed overnight at 4°C, then cryoprotected in 20% sucrose in 0.1 M phosphate buffer. Longitudinal sections were obtained (15 µm) and processed for immunostaining to determine the regional and cellular specificity of EGFP. Sections were thaw-mounted onto glass slides, permeabilized in cold acetone (−20°C for 10 min) and incubated at room temperature with blocking solution [5% bovine serum albumin (BSA) containing 0.5% Triton™ X-100] for 1 h and incubated overnight at 4°C with primary antibodies: mouse monoclonal antibodies against myc (1:100, Santa Cruz), MOG (Dr Sara Piddlesden, Cardiff, 1:50), GFAP (Invitrogen, 1:400), NeuN (Chemicon, 1:400), CC-1 (Calbiochem, 1:50), Cx43 (Invitrogen, 1:200), MBP (Abcam, 1:500); rabbit antisera against Cx47 (clone 935, 1:800) (Orthmann-Murphy *et al.*, 2007*a*), EGFP (Invitrogen, 1:2000), Iba1 (Biocare, 1:500), Caspase-3 (Millipore, 1:20), Cx30 (Invitrogen, 1:300), Olig2 (Millipore, 1:300); and rat anti-CD68 (Serotec, 1:100) and anti-F4/80 (Serotec, 1:50). Sections were then washed and incubated with appropriate secondary antibodies (Jackson ImmunoResearch) for 1 h at room temperature. Cell nuclei were visualized with 4′,6′-diamidino-2-phenylindole (DAPI; Sigma-Aldrich). Slides were mounted with Dako Fluorescent Mounting Medium and photographed under a Zeiss fluorescence microscope (Carl Zeiss MicroImaging).

Quantification of viral spread

To assess the intracranial vector spread and AAV-mediated transgene expression we examined AAV.MBP.EGFP injected wild-type mice at postnatal Day 30, 3 weeks following vector delivery at postnatal Day 10 ($n = 5$ mice) by counting the area of GFP expression using a modified method adapted from previous studies (von Jonquieres *et al.*, 2013). Sagittal brain sections spaced 90–450 µm apart (with smaller intervals near the injection site) were taken at ×10 magnification and the total area of GFP expression was determined based on hand-drawn maps and dimensions determined by the Mouse Brain Atlas in stereotactic coordinates (Franklin and Paxinos). Results for each sagittal section were plotted in Excel and averaged between mice. The volume of the vector spread was estimated as the sum of all interval volumes calculated by multiplying the average area of GFP immunoreactivity of two successive sections by the sampling interval between them. Additionally, we examined vector spread in the cervical spinal cord. The percentage of GFP+ oligodendrocytes was measured in the corpus callosum, in the internal capsule, ventral pons/corticospinal tract area and cervical spinal cord anteriolateral white matter.

Analysis of Cx47 expression

The expression of Cx47 in postnatal Day 30 Cx47 knockout mice injected with AAV.MBP.Cx47myc at the age of postnatal Day 10 was analysed by immunostaining with anti-Cx47 and anti-myc antibodies. The numbers of Cx47-expresing cells were counted in the corpus callosum, in the internal capsule, ventral pons/corticospinal tract area and cervical spinal cord anteriolateral white matter in images taken from sections double-stained with cell markers (as above). We calculated the percentage of Cx47-expressing oligodendrocytes in at least three different sections per mouse from $n = 5$ mice. The percentages of Cx47+ astrocytes and neurons were measured in the corpus callosum and in the internal capsule.

In addition, we quantified gap junction formation by Cx47 in at least 20 randomly captured individual oligodendrocytes within an area of 28.75 µm^2 from corpus callosum as well as from the internal capsule areas from $n = 5$ AAV.MBP.Cx47myc injected Cx47 knockout mice in pictures captured at ×200 magnification. The total number of Cx47 gap junction plaques in each image were counted using Adobe Photoshop 6. For comparison, we counted the number of Cx47 gap junction plaques in oligodendrocytes of $n = 2$ wild-type mice in the same areas.

Experimental design of treatment trial in Cx32/Cx47 double knockout mice

We performed a treatment trial with stereotactic injection of the AAV.MBP.Cx47myc (fully treated group, $n = 22$) or of the AAV.MBP.EGFP vector (mock treated group, $n = 18$) in the internal capsule of the left hemisphere of postnatal Day 10 (weighing 5–6 g) Cx32/Cx47 double knockout littermate mice. We also used $n = 17$ untreated littermate double knockout mice as additional control group. Mice were randomized to the treatment groups and all subsequent analysis of behaviour and pathology was performed blinded to the treatment condition. However, blinding was not possible in immunofluorescence studies because only mock-vector injected animals showed intense AAV-driven EGFP expression in

oligodendrocytes above the baseline transgenic EGFP expression seen in the Cx47 knockout line. Most mice were observed until postnatal Day 30 (3 weeks after injection), at which point behavioural testing was performed as a primary experimental outcome, followed by either pathological analysis (immunostaining, immunoblot, morphometric analysis) as a secondary experimental outcome. For immunostaining we evaluated fully and mock treated mice ($n = 5$ per treatment group), for western blot we examined $n = 3$ fully treated and $n = 3$ untreated mice, for morphometric analysis of myelination we used fully and mock treated mice ($n = 5$ mice per group) along with wild-type mice as control ($n = 4$), and for dye transfer studies we used $n = 4$ fully treated mice and $n = 5$ untreated mice. Mice used for pathological analysis were previously subjected to behavioural testing along with $n = 9$ additional untreated littermate mice. Mice used for dye transfer studies were transferred to a collaborating lab at the age of postnatal Day 20 and did not undergo behavioural testing. Additional $n = 5$ treated and $n = 7$ mock-treated mice were observed beyond 30 days of age and until death in order to assess survival rates in each treatment group (Supplementary Fig. 1).

Behavioural analysis

To assess motor performance of treated mice we used the Foot slip test, the rotarod analysis, and the foot print analysis as previously described (Schiza *et al.*, 2015). One-month-old (postnatal Day 30) double knockout mice from all treatment groups (fully treated, mock treated, untreated) were examined in the home cage and at the same time of the day (9 a.m.) by an examiner blinded to the treatment condition.

For the Foot slip test (Britt *et al.*, 2010), which is considered sensitive for CNS demyelination models, mice were placed in a 15 × 15 × 15 cm clear plexiglass box with a floor consisting of a metal wire grid with 1.25 cm spacing with a 1.25 cm grid suspended 1.25 cm above the floor. Mice were acclimated in the box for 1 h before each session. The trial consisted of 50 steps. If a misstep results in the hindlimb or forelimb falling through the grid but the limb is withdrawn prior to touching the floor is scored 1; if the limb touches the floor it is scored 2. A video camera was used to film the mice to ensure accurate counts, and video recordings were evaluated in slow motion.

For the rotarod analysis, the apparatus consists of a computer-controlled, motor-driven rotating spindle and four lanes for four mice. One-month-old mice were habituated to the apparatus the first day for 180 s sessions twice at constant speeds of 12 and 20 rpm. The mean latency to fall off the rotarod was calculated.

In the footprint analysis, footprints were obtained by painting the paws with non-toxic coloured inks and the mouse was allowed to walk down a narrow, open-top runway covered with white paper. The runway length was 22 cm long and 10 cm wide. Furthermore, the open-top runway was flanked by two walls at each side that were 11 cm high. The mice were acclimatized to the environment for at least 60 min, and were allowed two practice runs before colouring the paws. To facilitate subsequent analysis, forelimbs and hindlimbs were coloured with different colours: blue for the front and red for the hindlimbs. Each mouse was subjected to a total of nine trials (three trials per day for 3 days). Once the footprints had dried, the following parameters were measured: overlap width, forelimb stride length, and hindlimb stride length for the left and right limbs separately.

Morphometric analysis of myelination

For semithin sections, 1-month-old fully treated and mock treated ($n = 5$ mice per group) littermate Cx32/Cx47 double knockout mice, as well as 1-month-old wild-type mice as controls ($n = 4$) were transcardially perfused with 2.5% glutaraldehyde in 0.1 M phosphate buffer. The cerebrum at the level of the corpus callosum and internal capsule, as well as the cervical spinal cord were dissected and further fixed overnight at 4°C, then osmicated, dehydrated, and embedded in Araldite® resin. Transverse semithin sections (1 µm) were obtained and stained with alkaline toluidine blue. The CNS myelin fraction was calculated within the corpus callosum, internal capsule and cervical spinal cord white matter in semithin sections using a modified method to estimate the density of myelinated fibres and myelin sheaths (Tang and Nyengaard, 1997; Sutor *et al.*, 2000; Vavlitou *et al.*, 2010). Images of semithin sections captured at ×630 final magnification following the same processing and microscopy settings were imported into Photoshop 6 (Adobe Systems) and a transparent counting grid was placed on the image. All intersections of the grid lines hitting myelinated fibres and myelin sheaths were counted separately. The volume density of the myelinated fibres in the white matter was calculated by the total number of points hitting myelinated fibres in the white matter over the total number of points hitting white matter area.

Immunoblot analysis

Fresh tissue samples were collected from the cerebrum at the level of the corpus callosum and lysed in ice cold RIPA buffer [10 mM sodium phosphate pH 7.0, 150 mM NaCl, 2 mM EDTA, 50 mM sodium fluoride, 1% NP-40, 1% sodium deoxycholate and 0.1% sodium dodecyl sulphate (SDS)] containing a cocktail protease inhibitors (Roche). Tissues were sonicated and protein concentrations were measured on a NanoDrop. Fifty micrograms of protein from each tissue lysate were loaded into each well and fractioned by 12% SDS-poly acrylamide gel electrophoresis gel. Proteins were transferred to a Hybond-C extra membrane (GE Healthcare Bio-Sciences), using semidry transfer unit. Non-specific sites on the membrane were blocked with 5% non-fat milk in Tris-buffered saline containing 0.1% Tween 20 (TBS-T) for 1 h at room temperature. Immunoblots were then incubated with rabbit antisera against Cx47 (1:500, a kind gift of Prof. Klaus Willecke, University of Bonn) (May *et al.*, 2013), or against EGFP (1:1000, Abcam); or with mouse monoclonal antibodies against myc (1:500, Santa Cruz) and MBP (1:2000, Abcam) in 5% milk and TBS-T, at 4°C overnight. After washing, immunoblots were incubated with anti-rabbit or anti-mouse horseradish peroxidase-conjugated secondary antiserum (Jackson ImmunoResearch Laboratories, 1:3000) in 5% milk-TBS-T, for 1 h. Membranes were then reblotted with GAPDH (Santa Cruz, 1:4000) or with tubulin (E7, DSHB, 1:3000) antibodies as a loading control. The bound antibody was visualized by enhanced chemiluminescence system (ECL Plus, GE Healthcare Bio-Sciences, Amersham). To compare myelin protein levels between samples, band intensity was measured using TinaScan software version 2.07d.

Analysis of white matter pathology by immunostaining

To assess the amount of inflammation and astrogliosis in the corpus callosum and cervical spinal cord of treated compared to mock-treated mice we counted using ImageJ software the total immunofluorescence for Iba1, a microglia marker, and GFAP, an astrocyte marker, respectively, and compared the ratios of total area covered by Iba1 or GFAP immunofluorescence. We also counted the number of CD68 or F4/80 stained macrophages per section. To quantify the extent of oligodendrocyte apoptosis we double stained sections with oligodendrocyte marker CC-1 and apoptosis marker caspase-3, and counted the percentage of caspase-3 positive oligodendrocytes. Olig2 + oligodendrocyte precursor cells were also counted in the corpus callosum. For each quantification multiple microscope pictures were taken from the corpus callosum or cervical spinal cord from at least three immunostained sections per mouse and results were averaged per mouse in $n = 5$ mice per treatment group.

Dye transfer experiments

Mice were decapitated under anaesthesia. The brain was removed immediately and placed in ice cold, oxygenated (95% O_2/5% CO_2) artificial CSF containing (in mM): 125 NaCl, 3.5 KCl, 26 $NaHCO_3$, 1 $MgCl_2$ and 10 glucose (pH 7.4, 315 mOsm/l). The brain was blocked and glued onto the stage of a vibratome (Leica, VT1000S). Brain slices (200-µm thick) containing the corpus callosum were taken and transferred to a submerged chamber, which was continuously superfused with oxygenated (95% O2/5% CO2) artificial CSF containing (mM): 125 NaCl, 3.5 KCl, 26 $NaHCO_3$, 2 $CaCl_2$, 1 $MgCl_2$ and 10 glucose (pH 7.4, 315 mOsm/l) at room temperature. The slices were allowed to equilibrate for at least 1 h in this chamber before experiments began. Slices were then transferred to a submerged recording chamber, which continuously superfused oxygenated (95% O2/5% CO2) artificial CSF containing (in mM): 125 NaCl, 3.5 KCl, 26 $NaHCO_3$, 2 $CaCl_2$, 1 $MgCl_2$ and 10 glucose (pH 7.4, 315mOsm/l) at room temperature.

Oligodendrocytes were identified both with differential interface contrast (DIC) optics and fluorescence for GFP with an Axioskop2 microscope (Supplementary Fig. 2). Images were digitized with a monochrome camera and the SCIght software (Scientifica, Ltd). An oligodendrocyte was first identified with fluorescent imaging and then impaled with patch pipettes from borosilicate glass filled with the intracellular solution containing (in mM): 120 K-gluocanate, 15 HEPES, 2 KCl, $MgCl_2$, 3 NaATP, 0.3 NaGTP, lucifer yellow (0.1%), pH 7.3, 290 mOsm. Responses were amplified using a Axopatch-200B amplifier, digitized using the ITC-18 board (Instrutech, Inc) on a PC running IgorPro software (Wavemetrics, Inc) (Fig. 7B).

Data were acquired and analysed using custom-written procedures in IgorPro software (Wavemetrics, Inc). Throughout the experiment, the membrane voltage was stepped from −70 mV to +40 mV in 10 mV step increments and membrane currents were recorded. Fluorescent images for Lucifer yellow were monitored continuously throughout the experiment to ensure intracellular access and dye transfer. Each oligodendrocyte was monitored for at least 30 min. Only one recording from each brain slice was performed. We counted the number of coupled cells after each injection, as well as the percentage of injected cells showing network connection in each group.

Statistical analysis

Results of all behavioural studies and survival rates were compared using the Mann-Whitney U-test. For all other comparisons we used the unpaired two-tailed Student's *t*-test. Significance was defined as $P < 0.05$ in all comparisons.

Results

The AAV.MBP vector leads to widespread oligodendrocyte-specific expression

The AAV.MBP.EGFP (mock) and AAV.MBP.Cx47myc (full) plasmids (Fig. 1A and B) were successfully cloned and showed high expression in transfected AAV-293 cells. Following AAV packaging, the vector titres obtained ranged from 10^{12} to 9.5×10^{12} genome copies/ml as determined by quantitative PCR and from 9×10^{11} to 5.83×10^{12} capsids/ml as estimated by the quantitative AAV ELISA. We injected stereotactically the AAV vectors in the internal capsule area in groups of postnatal Day 10 mice. The injections did not cause any lasting widespread inflammatory responses as indicated by immunostaining of brain sections with lymphocyte (CD3, CD20) and macrophage (CD68) markers. Only small numbers of inflammatory cells were seen at the immediate site of injection 3 weeks later (data not shown).

We examined the distribution of EGFP expression following injection of the AAV.MBP.EGFP vector into the internal capsule area of the left hemisphere. At postnatal Day 30 we detected a maximum of EGFP positive cells in the corpus callosum and the internal capsule (Fig. 1C–F), while further areas showing partial expression included the striatum, hippocampus, midbrain, superficial layers of the pons, olfactory bulb, and basal forebrain (Supplementary Fig. 3). Viral expression extended also to the contralateral right hemisphere including the corpus callosum. Furthermore, EGFP expression was detected in extensive white matter areas of the cervical and thoracic spinal cord (Supplementary Fig. 4). Calculation of intracranial expression area from $n = 5$ injected mice showed a wide distribution of the AAV expression (Fig. 1G). The maximum rostro-caudal spread of EGFP expression was 7.61 ± 0.68 mm, and the maximum lateral spread was 4.61 ± 0.66 mm. The total expression volume including both hemispheres was 46.00 ± 7.93 mm^3. Immunoblot analysis confirmed EGFP expression at higher levels in the injected left compared to the contralateral right cerebral hemisphere, but also at lower levels in further CNS areas

including the olfactory bulb, cerebellum and spinal cord (Fig. 1H). Expression rates in mature oligodendrocytes ranged from 74.86 ± 13.17% in the corpus callosum, 73.73 ± 14.86% in the internal capsule, 44.08 ± 16.45% in the ventral pons, and 49.02 ± 12.48% in cervical spinal cord anteriolateral white matter (Fig. 1I). EGFP expression was found also in Olig2+ oligodendrocyte precursor cells but at lower rates than in mature oligodendrocytes (in the corpus callosum: 41.99 ± 7.15%; in the internal capsule: 34.67 ± 8.49%). EGFP was only expressed in oligodendrocyte linage cells labelled with CC1 or Olig2 but not in NeuN+ neurons, in GFAP+ astrocytes, or in Iba1+ microglia (Fig. 1J–M).

AAV.MBP.Cx47myc vector leads to expression of Cx47 and gap junction plaque formation specifically in oligodendrocytes

Following injection of the AAV.MBP.Cx47myc vector in the internal capsule area of Cx47 knockout postnatal Day 10 mice, we examined the expression of Cx47 3 weeks later by immunostaining and immunoblot analysis. Similar to the expression of the mock vector (above), widespread expression of Cx47 was detected in a high percentage of cells in the internal capsule and corpus callosum. Further expression was also detected in subsets of oligodendrocytes in the striatum, hippocampus, olfactory bulb, midbrain, and superficially in the pons, as well as in the cervical and thoracic spinal cord. Virally expressed Cx47 showed the characteristic formation of GJ-like plaques in the cell bodies and proximal processes of oligodendrocytes, identified by their transgenically-derived low level GFP signal (Supplementary Figs 5–8) or by double staining with oligodendrocyte marker CC1 (Fig. 2). Cx47 gap junction plaques were immunoreactive for both Cx47 and myc, while neither Cx47 nor myc immunoreactivity were detectable in untreated Cx47 knockout mice. Cx47 expression was found only in EGFP or CC1 immunoreactive oligodendrocytes, but not in neurons (NeuN+), in astrocytes (GFAP+) or in microglia (Iba1+) (Fig. 2G–I). Quantification of the ratios of Cx47 expressing cells identified by cell markers in $n = 5$ AAV.MBP.Cx47myc injected mice confirmed high expression rates in oligodendrocytes in the corpus callosum (41.56 ± 4.5%) and in the internal capsule (31.78 ± 7.53%), but also in the ventral pons (42.27 ± 6.18%) and cervical spinal cord white matter (40.72 ± 7.65%) (Fig. 2J).

In the areas of AAV-mediated Cx47 expression numerous gap junction plaques were formed by Cx47, which appeared increased in individual oligodendrocytes compared to wild-type brain (Supplementary Fig. 8). Counts of Cx47 immunoreactive gap junction plaques per oligodendrocyte within the internal capsule and corpus callosum of AAV.MBP.Cx47myc injected Cx47 knockout mice ($n = 5$) were 51.91 ± 6.23 Cx47 gap junction plaques/oligodendrocyte in the corpus callosum (compared to 24.8 ± 0.1 in wild-type mice, $P = 0.048$) and 42.74 ± 2.83 in the internal capsule (compared to 25.3 ± 3.9 in wild-type mice, $P = 0.019$) (Fig. 2K). These results indicate that AAV-mediated Cx47 expression in individual oligodendrocytes was higher compared to physiological expression. However, the virally derived expression of Cx47 did not have any apparent effect on the expression of Cx32 in postnatal Day 30 Cx47 knockout mice (Supplementary Fig. 9).

The expression of Cx47 in Cx47 knockout mice injected with AAV.MBP.Cx47myc was also confirmed by immunoblot analysis in brain samples taken from the corpus callosum area using both anti-Cx47 as well as anti-myc antibodies (Fig. 2L and M). To further examine whether virally expressed Cx47 forms gap junction channels with its main astrocytic partner Cx43 (Altevogt and Paul, 2004; Kamasawa *et al.*, 2005; Orthmann-Murphy *et al.*, 2007*b*, 2009), we double stained brain sections from full vector injected Cx47 knockout mice for Cx47 and Cx43. We found co-localization of Cx47 and Cx43 immunoreactivity in gap junction plaques surrounding oligodendrocytes, indicating the formation of oligodendrocyte-astrocyte gap junctions mediated through the AAV expressed Cx47 (Supplementary Fig. 10). In contrast, Cx47 expressed in grey matter oligodendrocytes did not co-localize with astrocytic Cx30, which physiologically does not form gap junction channels with Cx47 (Altevogt and Paul, 2004; Kamasawa *et al.*, 2005; Orthmann-Murphy *et al.*, 2007*b*, 2009).

AAV.MBP.Cx47myc injected Cx32/Cx47 double knockout mice show improved motor performance, coordination, and survival

Having established widespread expression of our AAV.MBP vectors and high rates of oligodendrocyte-specific Cx47 expression in the cerebral white matter of Cx47 knockout mice, we proceeded with a treatment trial in Cx32/Cx47 double knockout mice, a model of hypomyelinating leukodystrophy. AAV.MBP.Cx47myc-injected Cx32/Cx47 double knockout mice showed improvement of symptoms that appear in untreated or mock-treated mice at one month of age, including tremor and impaired balance with gait dysfunction (Supplementary video). For behavioural analysis untreated (no vector injection), mock-treated (AAV.MBP.EGFP injection) and fully treated (AAV.MBP.Cx47myc injection) littermate mice were subjected to foot print test ($n = 9$ per group), foot slip test ($n = 9$–12 per group) and rotarod test ($n = 8$–10 per group). All parameters of foot print analysis, including stride length for all limbs and overlap width, were significantly improved in fully treated compared to untreated and mock treated double knockout mice (Fig. 3A–C).

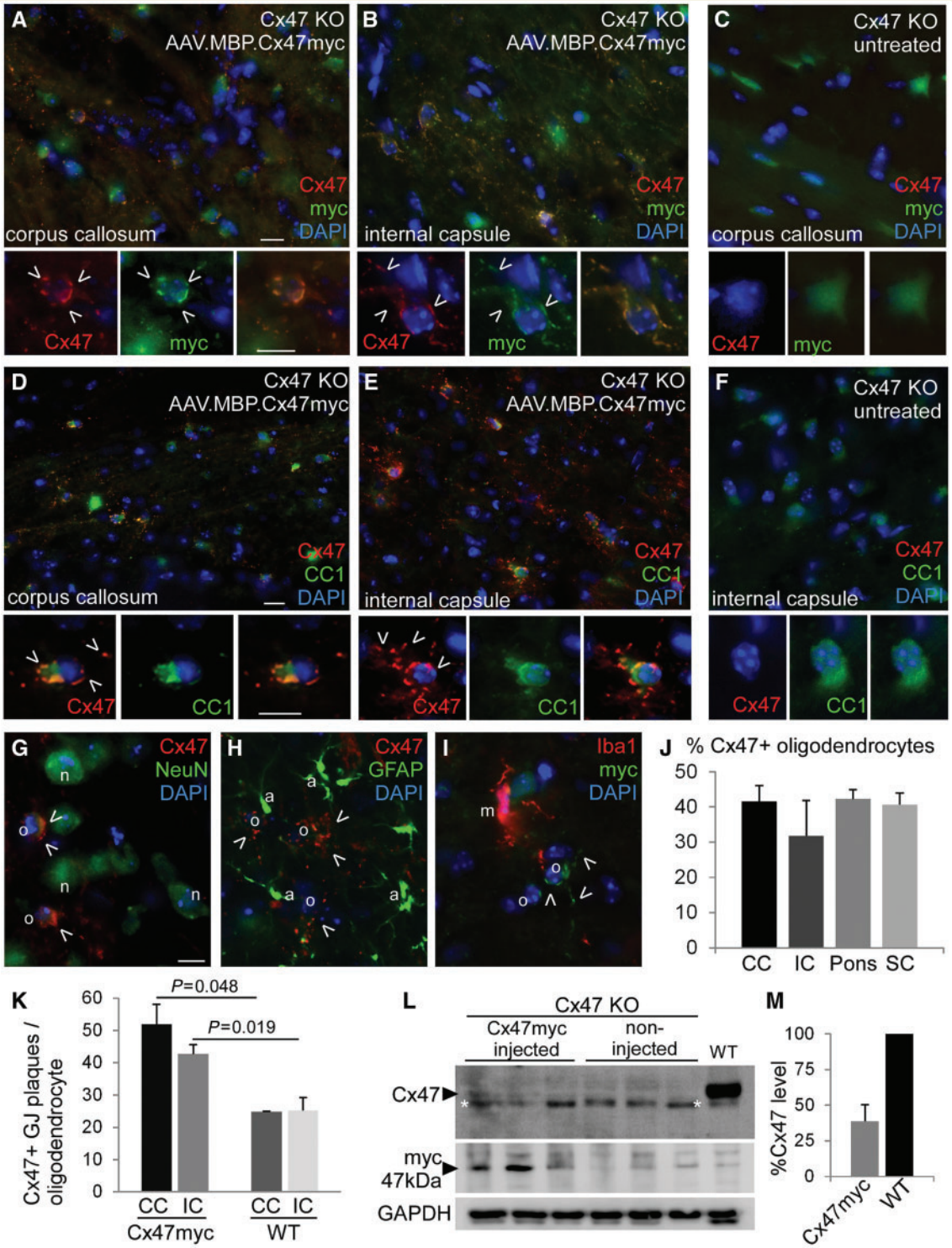

Figure 2 AAV.MBP.Cx47myc leads to expression of Cx47 and gap junction formation in oligodendrocytes of Cx47 knockout mice. Double immunostaining for Cx47 (red) and either the myc tag (**A–C**) or the oligodendrocyte marker CC1 (**D–F**) (green) shows Cx47 expression and formation of gap junction (GJ) like plaques (open arrowheads) at the pericarya and proximal processes of oligodendrocytes in the corpus callosum and internal capsule co-localizing with the myc immunoreactivity (**A** and **B**) and restricted to CC1 + oligodendrocytes in full vector injected mice, while untreated Cx47 knockout mouse brain shows no Cx47 or myc immunoreactivity (**C** and **F**). Some endogenous green fluorescence is present diffusely in the cytoplasm of all Cx47 knockout oligodendrocytes (including the untreated mice) due to the transgenic expression. Double immunostaining for Cx47 or myc and other cell markers including neuronal NeuN (**G**), astrocytic GFAP (**H**), and microglia Iba1 (**I**) confirms that Cx47 is not expressed in any of these cell types and is restricted to oligodendrocytes. Scale bars = 10 μm. (**J**) Quantification of the percentage of Cx47 expressing oligodendrocytes in the corpus callosum (CC), internal capsule (IC), ventral pons (corticospinal tract area) and cervical spinal cord (SC) anteriolateral white matter of *n* = 5 mice shows high expression ratios in all areas. (**K**) Counts of Cx47 gap junction

(continued)

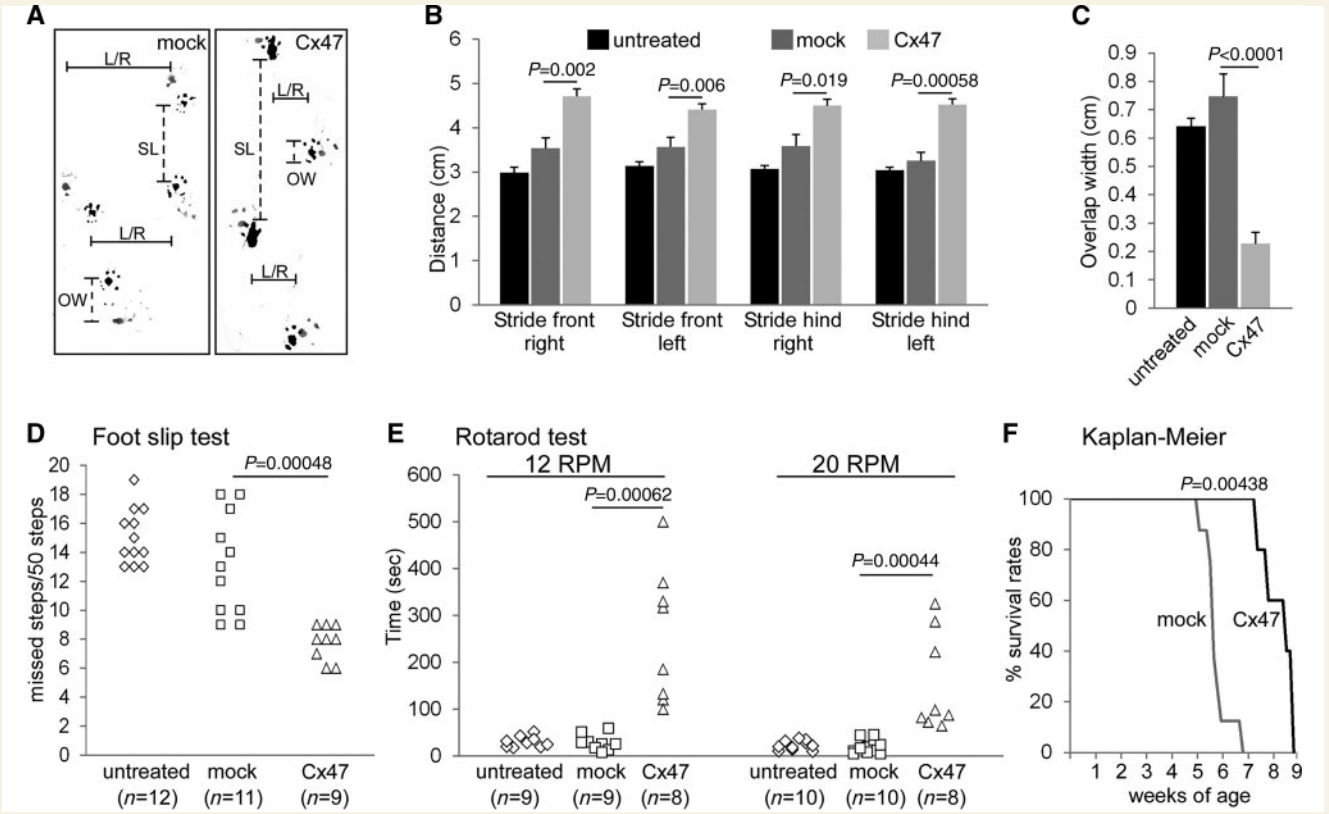

Figure 3 Improved motor performance and survival in AAV.MBP.Cx47myc injected Cx32/Cx47 double knockout mice. (**A**) Representative photographs of foot prints from a mock-treated (mock) mouse and from an AAV.MBP.Cx47myc treated (Cx47) mouse as indicated, shows increased stride length (SL) and reduced overlap width (OW) in the treated mouse, as well as improvement in the gait ataxia evident in the reduced distance between left and right foot prints (L/R). Quantitative foot print analysis in groups of untreated, mock-treated (with AAV.MBP.EGFP), and fully treated (with AAV.MBP.Cx47myc) mice (n = 9 per group) as indicated confirms significant improvement in all stride length parameters (**B**) as well as in overlap width (**C**) of treated mice. (**D**) Foot slip test shows fewer missed steps in fully treated compared to mock treated and untreated mice. (**E**) Rotarod analysis at 12 and 20 rotations per min (RPM) as indicated shows longer stay of treated mice on the rotarod. (**F**) Kaplan-Meier analysis of survival rates in mock-treated (n = 7) compared to fully treated mice (n = 5) shows a significant prolongation of survival in the treated group (41 ± 3.6 days in the mock group; 58 ± 4.7 days in the treatment group) (Mann-Whitney U-test for all comparisons; only significant P-values are shown).

Furthermore, the foot slip test revealed that treated double knockout mice had an average of 7.7 ± 1.2 (average ± SEM) missteps whereas mock treated double knockout mice had an average of 13.2 ± 3.5 missteps (P = 0.00048, Mann-Whitney U-test) (Fig. 3D). Finally, treated double knockout mice showed significant improvement in time spent on the rotarod at different speeds compared to mock treated mice (at 12 rpm: treated 256.8 ± 50.8 s and mock-treated 28.8 ± 5.5 s, P = 0.00062; at 20 rpm: treated 154.6 ± 37.6 s and mock-treated 18.5 ± 4.8 s, P = 0.00044) (Fig. 3E). Thus, behavioural analysis showed overall an improvement in motor performance and coordination in AAV.MBP.Cx47myc treated Cx32/Cx47 double knockout mice.

Finally, analysis of survival rates in additional groups of mock (n = 7) and fully treated mice (n = 5) observed beyond 30 days of age and until death, revealed significantly prolonged survival in treated (58 ± 4.7 days) compared to mock-treated mice (41 ± 3.6 days, P = 0.00438) (Fig. 3F).

Figure 2 Continued

plaques per oligodendrocyte confirm the re-establishment of oligodendrocyte gap junctions at levels above those of wild-type mouse brain. (**L**) Immunoblot analysis of brain lysates from three AAV.MBP.Cx47myc injected mice shows the presence of a faint Cx47 band that is absent from non-injected Cx47 knockout mice and is present in a wild-type mouse sample run as positive control (a non-specific band below the specific one is marked with asterisk). Blotting with a myc antibody also shows immunoreactivity in injected mice, which is absent from non-injected knockout and from the wild-type mouse. GAPDH blot is used for loading control. (**M**) Quantification of band intensity shows that Cx47 level in treated knockout mice reached 38.73 ± 11.69% of the wild-type brain sample. KO = knockout.

Improved myelination in AAV.MBP.Cx47myc injected Cx32/Cx47 double knockout mice

Cx32/Cx47 double knockout mice show significant demyelination, white matter vacuolation and oligodendrocyte apoptosis at 1 month of age (Menichella *et al.*, 2003; Odermatt *et al.*, 2003; Schiza *et al.*, 2015). To assess the effects of AAV-mediated Cx47 expression on this severe and early demyelination we examined toluidine-stained semithin sections (1 µm) of the cerebrum at the level of the corpus callosum and of the spinal cord anterior and posterior white matter at the cervical level in groups of treated and mock treated mice ($n = 5$ mice per group) along with wild-type mice of the same age ($n = 4$) as additional controls. The typical demyelinating pathology including loss of myelinated fibres, reduction of overall myelin density, and numerous large vacuoles was evident in mock-treated mice, whereas in AAV.MBP.Cx47myc treated animals there was significant preservation of the myelin structure and less vacuolation (Fig. 4A–R). To quantify these findings we measured the myelin volume density from multiple images ($n = 5$) per section and averaged the results per mouse. This analysis showed a significant improvement of myelin density in the corpus callosum and the internal capsule (Fig. 4S), as well as in the anterior and posterior spinal cord white matter (Fig. 4T) of treated compared to mock-treated mice, although this improvement did not reach the wild-type levels.

Improved inflammation, astrogliosis and oligodendrocyte apoptosis, in AAV.MBP.Cx47.myc injected Cx32/Cx47 double knockout mice

To examine whether AAV-mediated Cx47 gene replacement therapy could prevent the early and severe pathological changes that occur in Cx32/Cx47 double knockout CNS by 1 month of age (Menichella *et al.*, 2003; Odermatt *et al.*, 2003; Schiza *et al.*, 2015) we immunostained sections of the cerebrum at the level of the corpus callosum and of the cervical spinal cord from 1-month-old treated and mock-treated Cx32/Cx47 double knockout mice. Tissues were stained for macrophages markers CD68 or F4/80, for microglia marker Iba1, and for astrocyte marker GFAP. Numerous CD68 or F4/80 positive macrophages were detected in the corpus callosum area of mock-treated Cx32/Cx47 double knockout mice whereas treated mice showed significantly fewer macrophages, confirmed by counts performed in $n = 5$ mice per treatment group (in mock treated mice: 7.43 ± 0.87 macrophages per corpus callosum section; in fully treated mice 1.28 ± 0.61 macrophages per section, $P < 0.001$) (Fig. 5A–C and Supplementary Fig. 11). Likewise, treated mice showed a significant reduction in the number of macrophages in the anterior white matter of the cervical spinal cord (4.4 ± 1.78 per area examined compared to 11.06 ± 0.55 in mock-treated, $P < 0.0001$) (Supplementary Fig. 12).

Staining with Iba1 revealed marked activation of microglia in mock-treated mice, whereas in treated mice microglia-associated inflammation was ameliorated. Furthermore, astrogliosis shown by increased GFAP immunoreactivity in mock-treated mice was less pronounced in treated animals. Quantification of the amount of total Iba1 and GFAP immunofluorescence in $n = 5$ mice per group confirmed these findings both in the brain (Fig. 5D–G) and in the spinal cord (Supplementary Fig. 12).

In addition, myelin immunoreactivity was less disrupted in treated compared to mock-treated animals (Fig. 6A–D and Supplementary Fig. 12). To further corroborate these findings, we assessed the levels of myelin basic protein (MBP) by immunoblot analysis in brain lysates from treated and untreated mice ($n = 3$ per group) at postnatal Day 30. This analysis showed that MBP levels in fully treated double knockout mice were higher compared to untreated double knockout mice (Fig. 6E and F). Double labelling for oligodendrocytes with CC1 and caspase-3 showed in the corpus callosum area that a high percentage of oligodendrocytes in mock-treated Cx32/Cx47 double knockout mice where positive for this apoptotic marker ($50.29 \pm 11.13\%$), while apoptotic oligodendrocytes were much reduced in treated animals ($5.25 \pm 1.43\%$, $P = 0.0073$) (Fig. 6G–I). Significant reduction of apoptotic oligodendrocytes was also found in cervical spinal cord of treated mice (Supplementary Fig. 12). However, there was no significant difference in the total number of oligodendrocytes between the treatment groups (22.53 ± 9.96 CC1+ cells per area in treated; 23.2 ± 5.05 in mock treated). A non-significant trend for higher numbers of Olig2+ precursor cells was found in the corpus callosum of mock-treated mice (36.78 ± 12.46 Olig2+ cells per area compared to 29.73 ± 6.33 in treated mice; $P > 0.05$).

Re-establishment of oligodendrocyte network connectivity in AAV.MBP.Cx47myc treated double knockout mice

To demonstrate that the virally induced Cx47 expression in gap junction-deficient oligodendrocytes leads to functional coupling through gap junction channels, we examined gap junction-specific dye transfer in acute brain slices from 1-month-old treated and untreated Cx32/Cx47 double knockout mice. Oligodendrocytes were patch-clamped and recorded in the whole-cell configuration. The gap junction permeant dye Lucifer yellow was allowed to diffuse into the recorded cell (Supplementary Fig. 2). We used as positive control TG+Cx32/Cx47 double knockout mice (TG+) that have established gap junction connectivity through transgenic Cx32 expression in green fluorescent

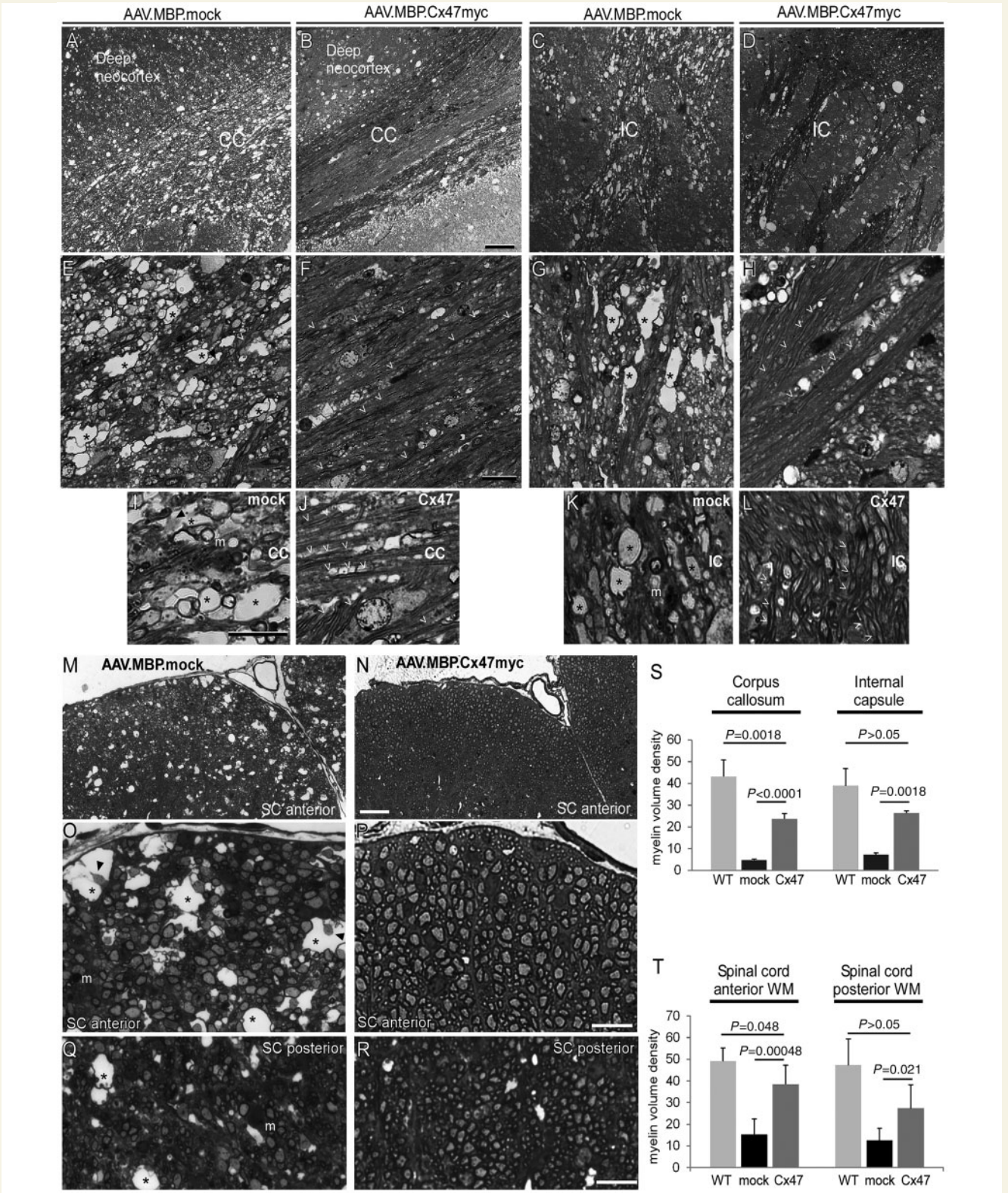

Figure 4 Improvement of myelin pathology in AAV.MBP.Cx47myc injected Cx32/Cx47 double knockout mice. Images of toluidine blue stained semithin brain (**A–L**) or spinal cord (SC) (**M–R**) sections from 1-month-old Cx32/Cx47 double knockout mice at the level of the corpus callosum (CC) at low (**A** and **B**) and higher magnification (**E**, **F**, **I** and **J**), as well as at the level of the internal capsule (IC) at low (**C** and **D**) and higher magnification (**G**, **H**, **K** and **L**), and at the cervical spinal cord level at low (**M** and **N**) and higher (**O–R**) magnification show a disrupted structure of the myelinated fibres in the corpus callosum, internal capsule and spinal cord anterior and posterior white matter (WM) of mock treated (mock) mice with reduced myelin density and vacuolation, whereas in AAV.MBP.Cx47myc injected mice (Cx47) the structure of myelin is better preserved and more dense. At higher magnification extensive vacuole formation (asterisks) is apparent in the mock treated mice, with only

(continued)

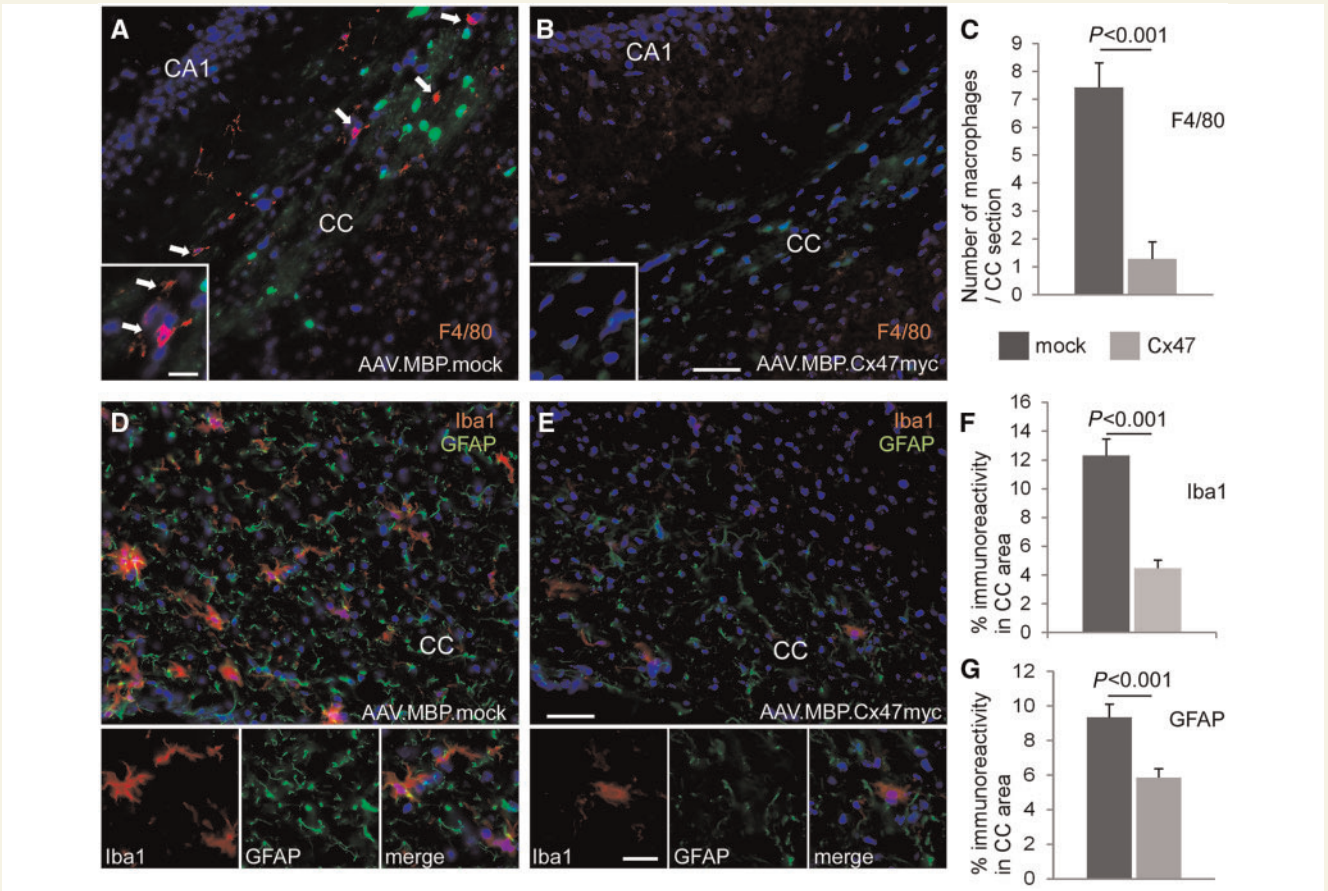

Figure 5 Improved inflammation and astrogliosis in AAV.MBP.Cx47myc treated Cx32/Cx47 double knockout mice.
Immunostaining for macrophage marker F4/80 (red) (**A** and **B**) shows numerous macrophages (arrows in **A**) in the corpus callosum (CC) area of the mock-treated mouse, while these are markedly reduced in the fully treated mouse (**B**). Green fluorescence in oligodendrocytes is derived from Cx47 knockout transgenic EGFP expression in both treatment groups, with additional and more intense green fluorescence in mock-treated brain due to AAV.MBP.EGFP expression. Cell nuclei are stained with DAPI throughout (blue). (**C**) Counts of macrophages in $n = 4$–5 sections per mouse in $n = 5$ mice confirm the significant reduction in numbers in the fully treated mice. (**D** and **E**) Immunostaining for microglia marker Iba1 (red) and astrocyte marker GFAP (green) shows in the fully treated mouse (**E**) marked improvement of microglial activation and astrogliosis seen in the mock treated brain (**D**). Quantification of total immunofluorescence for Iba1 (**F**) and GFAP (**G**) in $n = 5$ mice confirms these findings (Student's *t*-test for all comparisons). Scale bars = 50 μm in **A**, **B**, **D** and **E**; 10 μm in higher magnification insets.

oligodendrocytes (Schiza *et al.*, 2015), in which dye transfer in oligodendrocytes was evident. No significant dye transfer was observed in untreated double knockout used as a negative control. However, mice injected with the AAV.MBP.Cx47myc vector exhibited significant dye transfer similar to positive controls (Fig. 7), confirming that virally expressed Cx47 re-establishes gap junction coupling in oligodendrocytes of double knockout mice.

Discussion

The main goal of this study was to develop a targeted gene therapy approach for gene replacement specifically in oligodendrocytes. We achieved a widespread and highly cell specific expression using an AAV vector and an oligodendrocyte-specific promoter. This is the first time

Figure 4 Continued
a few intact myelinated fibres visible. In some of the vacuoles axonal remains can be seen (arrowheads), and myelin laden macrophages (m) are present (**E**, **G**, **I**, **K**, **O** and **Q**). In contrast, well-preserved numerous myelinated fibres (open arrowheads) are present in fully treated mice with only few vacuoles (**F**, **H**, **J**, **L**, **P**, and **R**). Scale bars = 50 μm in **A–D** and **M**–and **N**; 20 μm in **E–H** and **O–R**; 10 μm in **I–L**. Quantification of myelin density in the corpus callosum and internal capsule areas (**S**), as well as in the anterior and posterior spinal cord white matter (**T**) from $n = 5$ mice per treatment group confirms the significant improvement in myelination in fully treated compared to mock-treated mice, although myelin density does not reach the level of wild type (WT) mice ($n = 4$) of the same age (Student's *t*-test).

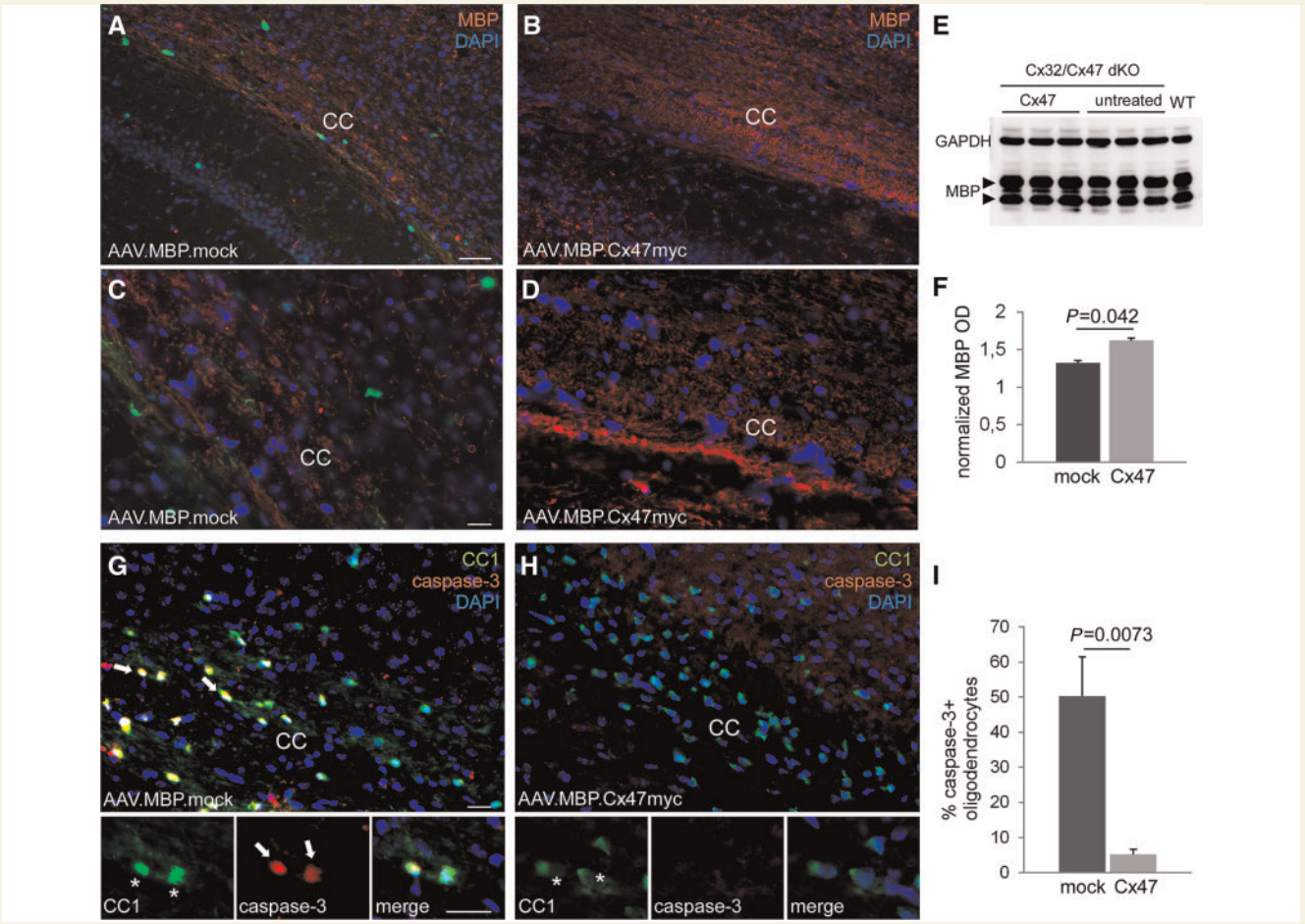

Figure 6 Improved myelination and reduced oligodendrocyte apoptosis in AAV.MBP.Cx47myc treated compared to untreated Cx32/Cx47 double knockout brain. (**A–D**) Images of brain sections at the level of the corpus callosum (CC) at low (**A** and **B**) and at higher (**C** and **D**) magnification, immunostained for myelin basic protein (MBP) (red) and counterstained with DAPI (blue). In the mock vector injected brain (**A** and **C**) intense green fluorescence derived from the AAV.MBP.EGFP vector is visible in numerous oligodendrocytes while MBP immunoreactivity is reduced compared to the fully treated (AAV.MBP.Cx47myc) brain (**B** and **D**). (**E** and **F**) Immunoblot analysis (blots of MPB and GAPDH for loading control shown in **E** and diagram with quantification of normalized band optic density intensity shown in **F**) of brain lysates from $n = 3$ mice per treatment group shows higher MBP levels in treated (Cx47) compared to untreated mice. Double staining of mock (**G**) and fully treated (**H**) mouse brain as indicated with oligodendrocyte marker CC1 (green) and apoptosis marker caspase-3 (red) shows several caspase-3 positive oligodendrocytes in mock treated brain but rare if any in the fully treated brain. (**I**) Counts of caspase-3-positive cells in $n = 5$ mice per treatment group confirms a significant reduction in the percentage of apoptotic oligodendrocytes in fully treated mice. *P*-values shown are from 2-tailed Student's *t*-test. Scale bars = 50 μm in **A** and **B**; 20 μm in **C**, **D**, **G** and **H**. dKO = double knockout.

AAV was used to target therapeutic expression of a myelin gene to oligodendrocytes. Using this approach in a relevant model of hypomyelinating leukodystrophy we demonstrate a significant behavioural, morphological and functional rescue of the severe early onset phenotype. Thus, we provide a proof of principle for a cell-specific somatic gene therapy approach to treat certain forms of leukodystrophy that result from mutations affecting structural proteins in myelinating cells.

Leukodystrophies are inherited disorders of CNS myelin with broad clinical manifestations and variable pathological mechanisms caused by mutations in numerous genes directly or indirectly involving oligodendrocytes (Helman *et al.*, 2015). Based on this genetic and neurobiological heterogeneity, many different approaches will be needed to develop future therapies. Certain forms that are caused by mutations in secreted proteins, including lysosomal storage diseases, may be corrected by expression of delivered genes in cell types other than oligodendrocytes, including neurons and astrocytes, taking advantage of the cross-correction mechanism (Lattanzi *et al.*, 2010, 2014). Furthermore, some leukodystrophies may be successfully treated by *ex vivo* gene therapy through cross-correction of dysfunctional oligodendrocytes via uptake of transgene products secreted by engineered haematopoietic stem cells (Cartier *et al.*, 2009; Biffi *et al.*, 2013).

However, achieving expression that is restricted to oligodendrocytes using cell-specific promoters is mandatory for

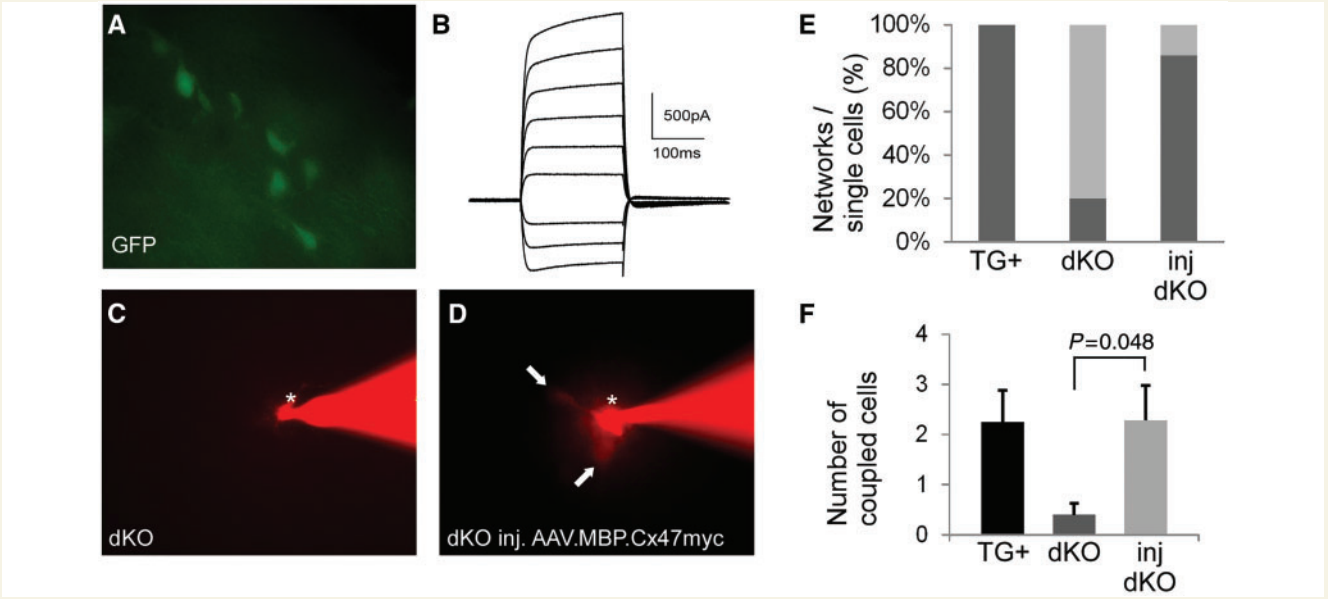

Figure 7 Re-establishment of oligodendrocyte network connectivity following Cx47 gene delivery with the AAV.MBP.Cx47myc vector. (**A**) Oligodendrocytes were identified by their transgenic expression of green fluorescence in all Cx32/Cx47 double knockout mice (see methods). (**B**) Representative membrane current recording from an oligodendrocyte. (**C** and **D**) Examples of Lucifer yellow (visualized red) injection into an oligodendrocyte (asterisk) in the corpus callosum in untreated double knockout mouse (**C**) and in an AAV.MBP.Cx47myc injected mouse (**D**). Whereas no transfer to another cell is noticed 30 min after injection in the double knockout, a red fluorescent signal in at least two adjacent cells (arrows) is observed in the treated mouse, suggesting establishment of network connectivity. Quantification of multiple experiments from positive control mice (TG + are double knockout expressing transgenically Cx32 in all oligodendrocytes, see methods) (n = 4 mice, four slices), from untreated double knockout mice (n = 5 mice, six slices) and from treated double knockout mice (n = 6 mice, six slices) shows that the percentage of network coupled oligodendrocytes per total cells (**E**) has markedly increased in the treated mice (85.7%), compared to 20% of untreated double knockout mice, and 100% of positive control TG + mice. (**F**) On average there is dye transfer to significantly more oligodendrocytes (number of couple cells) in treated (2.29 $\pm$ 0.69) compared to untreated (0.4 $\pm$ 0.690.23) mice (P = 0.048, unpaired Student t-test), reaching the levels of transgenic mouse network connectivity (2.25 $\pm$ 0.63). dKO = double knockout.

treatment of leukodystrophies caused by mutations in oligodendrocyte-specific structural proteins. Cx47, which is affected by loss-of-function mutations in patients with HLD2 (Uhlenberg *et al.*, 2004; Tress *et al.*, 2011) is expressed exclusively in oligodendrocytes in the CNS of rodents (Menichella *et al.*, 2003; Odermatt *et al.*, 2003), primates (Orthmann-Murphy *et al.*, 2007*a*), and humans (Sargiannidou *et al.*, 2008; Markoullis *et al.*, 2012, 2014), forming the majority of homotypic oligodendrocyte-oligodendrocyte as well as heterotypic oligodendrocyte-astrocyte gap junction channels (Menichella *et al.*, 2003; Odermatt *et al.*, 2003; Altevogt and Paul, 2004; Kleopa *et al.*, 2004; Kamasawa *et al.*, 2005; Orthmann-Murphy *et al.*, 2007*b*, 2009). The complexity and cell specific repertoire of connexin expression in CNS cells indicates that any ectopic expression in other cell types such as neurons or astrocytes could have unpredictable consequences for brain function. Astrocytes show a regionally highly specific pattern of connexin expression (Giaume *et al.*, 2010) and only certain populations of neurons are coupled by gap junctions to neighbouring cells in areas where coordinated function is needed, but not in other areas where they function independently. Furthermore, our previous studies using a transgenic approach to rescue the HLD2 model have supported a cell-autonomous disease mechanism in oligodendrocytes (Schiza *et al.*, 2015). Thus, it is crucial for any gene therapy approach to target specifically oligodendrocytes for treating HLD2 and similar types of leukodystrophies. This study provides the first successful somatic gene therapy approach to treat HLD2 preclinically.

Our approach using the *Mbp* promoter and vector delivery into the internal capsule at postnatal Day 10 resulted in oligodendrocyte-specific expression. Oligodendrocyte targeted gene delivery has been reported previously using the *Mbp* promoter in AAV vector (Chen *et al.*, 1999) and with the 2,3-cyclic nucleotide 3-phosphodiesterase (*Cnp*) promoter using a lentiviral vector (Kagiava *et al.*, 2014). As injection of a similar AAV vector with this *Mbp* promoter in neonatal brain at postnatal Day 0 resulted also in expression in astrocytes (von Jonquieres *et al.*, 2013), we chose for delivery a later developmental stage at postnatal Day 10, when MBP promoter leakage to non-oligodendrocyte linage cells is minimized. This time point proved to be sufficient for achieving a therapeutic benefit even in this HLD2 model with early onset severe CNS demyelination. Although in this study we examined expression up to postnatal Day 30, previous studies using the same AAV vector

showed a duration of expression similar to what has been shown for other AAV vectors, up to 270 dpi (von Jonquieres *et al.*, 2013). Thus, in future applications long lasting episomal expression in oligodendrocytes may be feasible after a single injection.

Despite the promising potential of the *Mbp* promoter used in this study (Mathis *et al.*, 2000; Forghani *et al.*, 2001) for clinical applications, there are potential limitations to its use including murine origin, relative big size and the poor specificity following neonatal vector delivery (von Jonquieres *et al.*, 2013). Although the 3.9 kb *Cnp* promoter (Gravel *et al.*, 1998; Sargiannidou *et al.*, 2009) has been successfully used for lentiviral gene delivery targeted to oligodendrocytes (Kagiava *et al.*, 2014), its relatively large size precludes the use in AAV vectors. A recently proposed alternative promoter for targeting AAV vectors to oligodendrocytes is the recombinant human myelin-associated glycoprotein (*MAG*) promoter (von Jonquieres *et al.*, 2016), which could also prove useful for developing leukodystrophy gene therapies.

Physiologically, Cx47 expression in rodents starts as early as at postnatal Day 7 and peaks around postnatal Day 14 (Teubner *et al.*, 2001), at least in the cerebellum, whereas cerebrum shows a later peak at postnatal Day 25 (Menichella *et al.*, 2003), slightly before the peak of myelination and expression of other myelin-related proteins including the other major oligodendrocyte connexin, Cx32 (Scherer *et al.*, 1995). However, in contrast to Cx47, Cx32 was not found to be expressed by oligodendrocyte precursor cells but only by mature oligodendrocytes (Markoullis *et al.*, 2012). This supports an earlier role of Cx47 in the oligodendrocyte linage, likely contributing to oligodendrocyte precursor cell differentiation, and explaining the hypomyelinating nature of HLD2 phenotype (Pouwels *et al.*, 2014). Expression of Cx47 in oligodendrocyte precursor cells has also been demonstrated in human brain under de- and remyelinating conditions (Markoullis *et al.*, 2012). The robust Cx47 expression achieved in this study both in mature oligodendrocytes and in their precursor cells by the AAV-mediated gene replacement at postnatal Day 10 was sufficient to prevent oligodendrocyte apoptosis, hypo- and demyelination, indicating that an early intervention during the beginning of myelination in the CNS would provide a therapeutic benefit in the clinical setting. Whether replacement of Cx47 at later disease stages and after the onset of pathology would be beneficial and to what degree remains to be shown.

Untreated and mock treated Cx32/Cx47 double knockout mice in this study showed the characteristic early leukodystrophy phenotype (Menichella *et al.*, 2003; Odermatt *et al.*, 2003) associated with severe demyelination, inflammation, astrogliosis and apoptosis of oligodendrocytes in the internal capsule and corpus callosum areas of the brain as well as in the spinal cord, where we focused our pathological analysis. Mock-treated mice showed no phenotypic difference compared to non-treated ones, suggesting that the injection process at postnatal Day 10 did not cause any lasting adverse effects. Fully treated Cx32/Cx47 double knockout showed a marked improvement in all behavioural studies focusing on motor function and coordination. Gait coordination and rotarod performance of AAV.MBP.Cx47myc injected mice was similar to PLP.Cx32 double knockout transgenic mice with expression of Cx32 throughout the CNS, including cerebellum and spinal cord (Schiza *et al.*, 2015), indicating that strong Cx47 oligodendrocyte expression even though restricted to certain white matter areas is sufficient to achieve significant—if not complete—functional rescue. However, Cx32 cannot fully replace the function of Cx47 in oligodendrocytes, as it is not compatible with astrocytic Cx43 (Altevogt and Paul, 2004; Orthmann-Murphy *et al.*, 2007*b*; Magnotti *et al.*, 2011). Therefore, it cannot fully rescue all the oligodendrocyte-astrocyte connections, especially in the white matter, where its astrocytic partner, Cx30, is normally not expressed (Markoullis *et al.*, 2012).

AAV expressed Cx47 co-localized with the astrocytic partner Cx43, indicating that gap junction connectivity to astrocytes is re-established. This oligodendrocyte-astrocyte connection is crucial for the homeostasis of oligodendrocytes and myelin, as demonstrated in relevant animal models (Lutz *et al.*, 2009; Tress *et al.*, 2012; May *et al.*, 2013), and in human disorders in which loss of Cx43 leads to leukodystrophy (Paznekas *et al.*, 2003). Moreover, we directly demonstrate that virally delivered Cx47 forms functional gap junction channels in oligodendrocytes, allowing the GJ-permeant dye transfer to other cells within the glial syncytium.

Detailed morphological analysis of AAV.MBP.Cx47myc treated mice demonstrated a significant rescue of myelination, with preservation of the myelin structure and prevention of vacuolation and demyelination. We focused our analysis on the brain areas where strong Cx47 expression was achieved, and found improved myelin density and almost complete prevention of oligodendrocyte apoptosis, as also shown in PLP.Cx32 double knockout mice (Schiza *et al.*, 2015). Furthermore, the associated inflammatory changes, including microglia activation, astrogliosis and macrophage infiltrates were effectively rescued.

Early gene delivery would be crucial for restoring oligodendrocyte function and myelination during development in hypomyelinating leukodystrophy forms (Pouwels *et al.*, 2014). Onset of HLD2 is typically in late infancy (Uhlenberg *et al.*, 2004; Bugiani *et al.*, 2006; Orthmann-Murphy *et al.*, 2009; Bilir *et al.*, 2013), indicating that gene delivery may need to be planned as early as possible for preventing the hypomyelinating leukodystrophy. Even earlier interventions, such as *in utero* or neonatal injection may be needed for other forms of leukodystrophy with early infancy onset, such as connatal Pelizaeus-Merzbacher disease or Canavan's disease.

Our study provides proof of principle for the effectiveness of oligodendrocyte-specific *GJC2*/Cx47 gene replacement to treat HLD2 using the AAV.MBP vector. It also provides an approach for treating other similar forms of

leukodystrophies. This approach will need to be validated in large animal models, and ultimately in clinical trials. AAV vectors have been recently shown to provide therapeutic benefit in other forms of leukodystrophy including globoid cell leukodystrophy (Lin *et al.*, 2015) and metachromatic leukodystrophy (Hironaka *et al.*, 2015). Although immunological reaction to the AAV vector delivery has been insignificant in our study and in other reports, there is a possibility of immunological reaction to the expressed protein (Hironaka *et al.*, 2015) limiting the duration of expression. This issue along with the distribution of the vector expression, which is more relevant for non-secreted gene products, as in our study, will need to be addressed in future studies.

Acknowledgements

We thank Prof. Angela Gritti (San Rafaelle Scientific Institute, Milan) for help with the initial development of the intracerebral injection method and for helpful discussions, and Prof. Klaus Willecke (University of Bonn) for the kind gift of the Cx47 antibody, as well as Marianna Nearchou for assistance in processing the semithin samples and Panayiota Pirpa for help with DNA sequencing. The antibody against tubulin-E7 (developed by Michael Klymkowsky) was obtained from the Developmental Studies Hybridoma Bank developed under the auspices of the National Institute of Child Health and Human Development and maintained by Department of Biology, The University of Iowa, Iowa City.

Funding

This work was funded by the European Leukodystrophy Association (ELA) Research Foundation (ELA 2011-025I2 grant to K.A.K.) and also supported by the National Multiple Sclerosis Society (RG459A1/2 grant to K.A.K.) and by the Muscular Dystrophy Association (Grant 277250 to KAK).

Supplementary material

Supplementary material is available at *Brain* online.

References

Ahn M, Lee J, Gustafsson A, Enriquez A, Lancaster E, Sul J, et al. Cx29 and Cx32, two connexins expressed by myelinating glia, do not interact and are functionally distinct. J Neurosci Res 2008; 86: 992–1006.

Altevogt BM, Kleopa KA, Postma FR, Scherer SS, Paul DL. Connexin29 is uniquely distributed within myelinating glial cells of the central and peripheral nervous systems. J Neurosci 2002; 22: 6458–70.

Altevogt BM, Paul DL. Four classes of intercellular channels between glial cells in the CNS. J Neurosci 2004; 24: 4313–23.

Biffi A, Montini E, Lorioli L, Cesani M, Fumagalli F, Plati T, et al. Lentiviral hematopoietic stem cell gene therapy benefits metachromatic leukodystrophy. Science 2013; 341: 1233158.

Bilir B, Yapici Z, Yalcinkaya C, Baris I, Carvalho CM, Bartnik M, et al. High frequency of GJA12/GJC2 mutations in Turkish patients with Pelizaeus-Merzbacher disease. Clin Genet 2013; 83: 66–72.

Britt JM, Kane JR, Spaeth CS, Zuzek A, Robinson GL, Gbanaglo MY, et al. Polyethylene glycol rapidly restores axonal integrity and improves the rate of motor behavior recovery after sciatic nerve crush injury. J Neurophysiol 2010; 104: 695–703.

Bugiani M, Al Shahwan S, Lamantea E, Bizzi A, Bakhsh E, Moroni I, et al. GJA12 mutations in children with recessive hypomyelinating leukoencephalopathy. Neurology 2006; 67: 273–9.

Cartier N, Hacein-Bey-Abina S, Bartholomae CC, Veres G, Schmidt M, Kutschera I, et al. Hematopoietic stem cell gene therapy with a lentiviral vector in X-linked adrenoleukodystrophy. Science 2009; 326: 818–23.

Chen H, McCarty DM, Bruce AT, Suzuki K. Oligodendrocyte-specific gene expression in mouse brain: use of a myelin-forming cell type-specific promoter in an adeno-associated virus. J Neurosci Res 1999; 55: 504–13.

Forghani R, Garofalo L, Foran D, Farhadi H, Lepage P, Hudson T, et al. A distal upstream enhancer from the myelin basic protein gene regulates expression in myelin-forming schwann cells. J Neurosci 2001; 21: 3780–7.

Garbern J, Cambi F, Shy M, Kamholz J. The molecular pathogenesis of Pelizaeus—Merzbacher disease. Arch Neurol 1999; 56: 1210–14.

Garbern JY. Pelizaeus-Merzbacher disease: genetic and cellular pathogenesis. Cell Mol Life Sci 2007; 64: 50–65.

Giaume C, Koulakoff A, Roux L, Holcman D, Rouach N. Astroglial networks: a step further in neuroglial and gliovascular interactions. Nat Rev Neurosci 2010; 11: 87–99.

Gravel M, DiPolo A, Valera PB, Braun PE. Four-kilobase sequence of the mouse CNP gene directs spatial and temporal expression of lacZ in transgenic mice. J Neurosci Res 1998; 53: 393–404.

Helman G, Van Haren K, Escolar ML, Vanderver A. Emerging treatments for pediatric leukodystrophies. Pediatr Clin North Am 2015; 62: 649–66.

Hironaka K, Yamazaki Y, Hirai Y, Yamamoto M, Miyake N, Miyake K, et al. Enzyme replacement in the CSF to treat metachromatic leukodystrophy in mouse model using single intracerebroventricular injection of self-complementary AAV1 vector. Sci Rep 2015; 5: 13104.

Hudson LD, Garbern JY, Kamholz JA. Pelizaeus-Merzbacher disease. In: Lazzarini RA, editor. Myelin biology and disorders. San Diego: Elsevier; 2004. p. 867–85.

Inoue K. PLP1-related inherited dysmyelinating disorders: Pelizaeus-Merzbacher disease and spastic paraplegia type 2. Neurogenetics 2005; 6: 1–16.

Kagiava A, Sargiannidou I, Bashiardes S, Richter J, Schiza N, Christodoulou C, et al. Gene delivery targeted to oligodendrocytes using a lentiviral vector. J Gene Med 2014; 16: 364–73.

Kamasawa N, Sik A, Morita M, Yasumura T, Davidson K, Nagy J, et al. Connexin-47 and connexin-32 in gap junctions of oligodendrocyte somata, myelin sheaths, paranodal loops and Schmidt-Lanterman incisures: implications for ionic homeostasis and potassium siphoning. Neuroscience 2005; 136: 65–86.

Kleopa KA, Orthmann JL, Enriquez A, Paul DL, Scherer SS. Unique distribution of gap junction proteins connexin29, connexin32, and connexin47 in oligodendrocytes. Glia 2004; 47: 346–57.

Lattanzi A, Neri M, Maderna C, di Girolamo I, Martino S, Orlacchio A, et al. Widespread enzymatic correction of CNS tissues by a single intracerebral injection of therapeutic lentiviral vector in leukodystrophy mouse models. Hum Mol Genet 2010; 19: 2208–27.

Lattanzi A, Salvagno C, Maderna C, Benedicenti F, Morena F, Kulik W, et al. Therapeutic benefit of lentiviral-mediated neonatal

intracerebral gene therapy in a mouse model of globoid cell leukodystrophy. Hum Mol Genet 2014; 23: 3250–68.
Lin DS, Hsiao CD, Lee AY, Ho CS, Liu HL, Wang TJ, et al. Mitigation of cerebellar neuropathy in globoid cell leukodystrophy mice by AAV-mediated gene therapy. Gene 2015; 571: 81–90.
Lutz SE, Zhao Y, Gulinello M, Lee SC, Raine CS, Brosnan CF. Deletion of astrocyte connexins 43 and 30 leads to a dysmyelinating phenotype and hippocampal CA1 vacuolation. J Neurosci 2009; 29: 7743–52.
Magnotti LM, Goodenough DA, Paul DL. Deletion of oligodendrocyte Cx32 and astrocyte Cx43 causes white matter vacuolation, astrocyte loss and early mortality. Glia 2011; 59: 1064–74.
Markoullis K, Sargiannidou I, Schiza N, Hadjisavvas A, Roncaroli F, Reynolds R, et al. Gap junction pathology in multiple sclerosis lesions and in normal appearing white matter. Acta Neuropathol 2012; 123: 873–86.
Markoullis K, Sargiannidou I, Schiza N, Roncaroli F, Reynolds R, Kleopa KA. Oligodendrocyte gap junction loss and disconnection from reactive astrocytes in multiple sclerosis gray matter. J Neuropathol Exp Neurol 2014; 73: 865–79.
Mathis C, Hindelang C, LeMeur M, Borrelli E. A transgenic mouse model for inducible and reversible dysmyelination. J Neurosci 2000; 20: 7698–705.
May D, Tress O, Seifert G, Willecke K. Connexin47 protein phosphorylation and stability in oligodendrocytes depend on expression of Connexin43 protein in astrocytes. J Neurosci 2013; 33: 7985–96.
Menichella DM, Goodenough DA, Sirkowski E, Scherer SS, Paul DL. Connexins are critical for normal myelination in the CNS. J Neurosci 2003; 23: 5963–73.
Nagy JI, Ionescu AV, Lynn BD, Rash JE. Coupling of astrocyte connexins Cx26, Cx30, Cx43 to oligodendrocyte Cx29, Cx32, Cx47: implications from normal and connexin32 knockout mice. Glia 2003; 44: 205–18.
Nave K-A, Boespflug-Tanguy O. Developmental defects of myelin formation: from X-linked mutations to human dysmyelinating diseases. Neuroscientist 1996; 2: 33–43.
Nelles E, Butzler C, Jung D, Temme A, Gabriel H-D, Dahl U, et al. Defective propagation of signals generated by sympathetic nerve stimulation in the liver of connexin32-deficient mice. Proc Natl Acad Sci USA 1996; 93: 9565–70.
Odermatt B, Wellershaus K, Wallraff A, Seifert G, Degen J, Euwens C, et al. Connexin 47 (Cx47)-deficient mice with enhanced green fluorescent protein reporter gene reveal predominant oligodendrocytic expression of Cx47 and display vacuolized myelin in the CNS. J Neurosci 2003; 23: 4549–59.
Orthmann-Murphy JL, Enriquez AD, Abrams CK, Scherer SS. Loss-of-function connexin47 mutations cause Pelizaeus-Merzbacher-like disease. Mol Cell Neurosci 2007a; 34: 629–41.
Orthmann-Murphy JL, Freidin M, Fischer E, Scherer SS, Abrams CK. Two distinct heterotypic channels mediate gap junction coupling between astrocyte and oligodendrocyte connexins. J Neurosci 2007b; 27: 13949–57.
Orthmann-Murphy JL, Salsano E, Abrams CK, Bizzi A, Uziel G, Freidin MM, et al. Hereditary spastic paraplegia is a novel phenotype for GJA12/GJC2 mutations. Brain 2009; 132: 426–38.
Paznekas WA, Boyadjiev SA, Shapiro R, Daniels O, Wollnik B, Keegan CE, et al. Connexin 43 (GJA1) mutations cause the pleiotropic phenotype of oculodentodigital dysplasia. Am J Hum Genet 2003; 72: 408–18.
Pouwels PJ, Vanderver A, Bernard G, Wolf NI, Dreha-Kulczewksi SF, Deoni SC, et al. Hypomyelinating leukodystrophies: translational research progress and prospects. Ann Neurol 2014; 76: 5–19.
Rash JE, Yasumura T, Dudek FE, Nagy JI. Cell-specific expression of connexins and evidence of restricted gap junctional coupling between glial cells and between neurons. J Neurosci 2001; 21: 1983–2000.
Salviati L, Trevisson E, Baldoin MC, Toldo I, Sartori S, Calderone M, et al. A novel deletion in the GJA12 gene causes Pelizaeus-Merzbacher-like disease. Neurogenetics 2007; 8: 57–60.
Sargiannidou I, Ahn M, Enriquez AD, Peinado A, Reynolds R, Abrams CK, et al. Human oligodendrocytes express Cx31.3: function and interactions with Cx32 mutants. Neurobiol Dis 2008; 30: 221–33.
Sargiannidou I, Vavlitou N, Aristodemou S, Hadjisavvas A, Kyriacou K, Scherer SS, et al. Connexin32 mutations cause loss of function in Schwann cells and oligodendrocytes leading to PNS and CNS myelination defects. J Neurosci 2009; 29: 4748–61.
Scherer SS, Deschênes SM, Xu Y-T, Grinspan JB, Fischbeck KH, Paul DL. Connexin32 is a myelin-related protein in the PNS and CNS. J Neurosci 1995; 15: 8281–94.
Schiza N, Sargiannidou I, Kagiava A, Karaiskos C, Nearchou M, Kleopa KA. Transgenic replacement of Cx32 in gap junction-deficient oligodendrocytes rescues the phenotype of a hypomyelinating leukodystrophy model. Hum Mol Genet 2015; 24: 2049–64.
Sutor B, Schmolke C, Teubner B, Schirmer C, Willecke K. Myelination defects and neuronal hyperexcitability in the neocortex of connexin 32-deficient mice. Cereb Cortex 2000; 10: 684–97.
Tang Y, Nyengaard JR. A stereological method for estimating the total length and size of myelin fibers in human brain white matter. J Neurosci Methods 1997; 73: 193–200.
Teubner B, Odermatt B, Guldenagel M, Sohl G, Degen J, Bukauskas FF, et al. Functional expression of the new gap junction gene connexin47 transcribed in mouse brain and spinal cord neurons. J Neurosci 2001; 21: 1117–26.
Tress O, Maglione M, May D, Pivneva T, Richter N, Seyfarth J, et al. Panglial gap junctional communication is essential for maintenance of myelin in the CNS. J Neurosci 2012; 32: 7499–518.
Tress O, Maglione M, Zlomuzica A, May D, Dicke N, Degen J, et al. Pathologic and phenotypic alterations in a mouse expressing a connexin47 missense mutation that causes pelizaeus-merzbacher-like disease in humans. PLoS Genet 2011; 7: e1002146. Epub 2011 Jul 7.
Uhlenberg B, Schuelke M, Ruschendorf F, Ruf N, Kaindl AM, Henneke M, et al. Mutations in the gene encoding gap junction protein alpha 12 (Connexin 46.6) cause Pelizaeus-Merzbacher-like disease. Am J Hum Genet 2004; 75: 251–60.
Vavlitou N, Sargiannidou I, Markoullis K, Kyriacou K, Scherer SS, Kleopa KA. Axonal pathology precedes demyelination in a mouse model of X-linked demyelinating/type I Charcot-Marie tooth neuropathy. J Neuropathol Exp Neurol 2010; 69: 945–58.
von Jonquieres G, Frohlich D, Klugmann CB, Wen X, Harasta AE, Ramkumar R, et al. Recombinant human myelin-associated glycoprotein promoter drives selective AAV-mediated transgene expression in oligodendrocytes. Front Mol Neurosci 2016; 9: 13.
von Jonquieres G, Mersmann N, Klugmann CB, Harasta AE, Lutz B, Teahan O, et al. Glial promoter selectivity following AAV-delivery to the immature brain. PloS One 2013; 8: e65646.
Wolf NI, Cundall M, Rutland P, Rosser E, Surtees R, Benton S, et al. Frameshift mutation in GJA12 leading to nystagmus, spastic ataxia and CNS dys-/demyelination. Neurogenetics 2007; 8: 39–44.